The Thesis for the Degree of Doctor of Science of Kyoto University

Characterization of Carbon Clusters and Their Hydrogenated Derivatives Studied by Time-of-Flight Mass Spectroscopy Using Single-Photon Ionization Technique

by

Yoshiyasu Kato

Laboratory of Molecular Spectroscopy
Division of Chemistry
Graduate School of Science
Kyoto University

Table of Contents

Introduction for the Thesis

Carbon clusters have long attracted interests in pure and applied sciences such as molecular spectroscopy, theoretical chemistry, and material sciences [1,2]. The importance of research on the structure and reactivity of smaller carbon clusters is ever growing in astrochemistry because the recent progress in spectroscopy over the microwave, infrared, and visible-ultraviolet regions has disclosed the existence of a variety of carbon chains and other carbonaceous particles in the space [3]. The characterization of these carbon-containing species is indispensable for the elucidation of the molecular evolution in the space.

In the material science also the progress in the research activity has been astoundingly remarkable since the epoch-making discovery of buckminsterfullerene C_{60} [4] and the development of technique for mass-production of C_{60} [5]. The discovery of carbon nanotubes (CNT), almost simultaneous with that of fullerenes [6], also has caused an explosive expansion of research activities in CNT science and technology [7,8]. Various technical modifications of these new carbon allotropes have already yielded some new functional materials for commercial uses.

The present status is such that the progress in application-oriented studies is so rapid that basic studies on elementary small carbon clusters tend to be a little behind relative to the former. The primary motivation of the present study by the author is to

remedy for the lag in basic research on the composite units of the above-mentioned allotropes, that is, smaller carbon clusters. These clusters include linear carbon chains, monocyclic and polycyclic carbon rings, closed-cage fullerenes, graphitic sheets, bowl-shaped isomers, and so on.

A weak point of the study on these smaller carbon clusters is that ordinary spectroscopic techniques for the precise determination of molecular structures are not applicable except for short linear chain and small planar ring clusters. Such experiments as gas phase ion-chromatography suggest that larger carbon clusters have several structural isomers [9,10], but detailed information on the structure cannot be obtained by such a bulk analysis.

The scarcity of information on the structure of carbon clusters is related to the fact that carbon clusters are produced by relatively rude experimental methods such as electrical discharge of acetylene and other hydrocarbons and resistive heating of graphite. It is considered that most carbon atoms in hot gases produced by such methods are in the forms of C, C_2 and C_3 with some longer linear chains [11–15]. Pieces of evidence suggest that in the gases produced by laser ablation of graphite there may be substantial amounts of monocyclic clusters in addition to the linear chains. Therefore, the ablation technique seems a viable method to form and characterize various isomeric clusters both linear and cyclic.

Laser ablation [16,17] has been widely used for the study of gases of metals and semiconductors of high melting points. This technique is applied to the carbon cluster also in the past two decades. For the analysis of cluster formation by laser ablation technique such detection methods as emission spectroscopy [18], fast imaging technique

[19,20], and mass-spectroscopy are utilized. In particular, mass-spectroscopy allows the determination of size distribution of clusters. It also allows the detection of non-emissive clusters.

However, in order for mass-spectroscopy to be useful for the study of neutral carbon clusters they must be ionized without decomposition beforehand, needless to say. In the past, ionization was effected mostly by multi-photon ionization with a high-flux lasers [21], which often caused fragmentation of nascent neutral clusters. To avoid the fragmentation lasers emitting photons of energy just above the ionization energy of target clusters should be favorable. In fact, such a one-photon ionization method was applied for the study of fullerenes whose ionization energies are relatively low so that fluorine (F_2) lasers of photon energy of 7.89 eV (=157 nm), for example [22–24], were just capable of ionizing fullerenes having ionization energies of around 8 eV [25] without significant decomposition of the fullerenes. As to the application of the one-photon ionization technique for the study of smaller carbon clusters it was prohibitive until recently because ionization energies of such clusters are higher than the photon energy of easily available lasers [26,27]. Just recently, however, the ninth harmonics of a Nd:YAG laser of an energy of 10.5 eV(=118 nm) [28,29] was applied to the study of carbon clusters of ionization energies having up to about 10 eV [30,31]. Thus, neutral clusters down to C_6 became possible to ionize gently without extensive fragmentation. In this thesis the author utilizes the same harmonics of a Nd:YAG laser to survey carbon clusters and their hydrogenated derivatives.

Another advantage of laser ablation technique is that it is possible to produce derivatives of carbon clusters easily with adding reactants, such as H_2 [24,32–35], D_2 [34], H_2O

[32,33], D_2O [32], N_2 [32,33], CH_3CN [32,33], NH_3 [32,33], NO [22] and SO_2 [22], in the buffer gases, or treating some impurities, e.g. KOH [21,23], to graphite. From those produced derivatives, the structure and reactivity of carbon clusters may be inferred to a certain degree. One may draw an analogy to organic chemists' "trapping technique" to get information on reaction intermediates. By combining single-photon ionization technique, more reliable evaluation of reaction products is attained. The carbon cluster derivatives such as polyacetylene $HC_{2n}H$ and cyanopolyynes $HC_{2n+1}N$ themselves are interesting from the viewpoint of interstellar chemistry because such carbon chain molecules are one of the abundant species in the space [36].

Because of the limitation of experimental studies on the elusive neutral carbon clusters quantum chemical computations to predict the structure provide useful information. This is particularly true in the case of clusters possible to have a number of isomeric structures. According to computations it is predicted that carbon clusters C_n with n being less than 9 prefer linear structures whereas those larger than C_{10} favor monocyclic structures [37–39]. In particular, clusters of the form of C_{4n+2} ($n \geq 2$) are predicted to possess stability due to the aromaticity [38–41]. In spite of these computational prediction, however, definite experimental evidence to confirm monocyclic stable structures has not yet been obtained, although circumstantial evidence for the cyclic structure is available from various types of experiments such as photoelectron spectroscopy of gaseous negative ions [42,43] and infrared spectroscopy of matrix-isolated clusters [44–47]. Previous mass spectroscopic studies of the author's group demonstrated that under a certain condition, C_{10}^- ions in particular are predominantly observed which suggests an extra stability of cyclic C_{10} [48].

With the above-stated background the present thesis reports new findings which are presented as in the following manner: in Chapter 1 the author reports the result of the time-of-flight mass-spectroscopic study on neutral carbon clusters produced by laser-ablation of graphite followed by a gentle one-photon ionization in the He buffer gas atmosphere. It is found that clusters of one and the same size and constitution split into two components, slow and fast, along the direction of drift towards the detector. Furthermore, the size distribution of C_n of the slower component is totally different from the hitherto known distribution pattern and results in the sole survival of C_{10} at longer intervals between the ablation and ionization pulses. The extreme stability of C_{10} is discussed intensively. In Chapter 2, the He gas used as the buffer gas in Chapter 1 is replaced with H_2 and D_2. As in the He buffer gas the ablated products of one and the same size and constitution split into a slow and a fast component. Similarly to the case of the He buffer gas in Chapter 1, the product of the type of $C_{2n}H_2$ supposed to be of a polyyne type survives at longer delay times. In Chapter 3 the result of time-of-flight mass-spectroscopic measurements for the atmosphere of both He and H_2 buffer gases is presented at an elevated detection sensitivity and spectroscopic resolution. The result reveals that the slower component observed and discussed in Chapters 1 and 2 is further split into two component, the implication of the splitting is argued.

References

1. W. Weltner, Jr. and R. J. Van Zee, Chem. Rev. **89**, 1713 (1989)
2. A. Van Orden and R. J. Saycally, Chem. Rev. **98**, 2313 (1998)
3. P. Ehrenfreund and S. B. Charnley, Annu. Rev. Astron. Astrophys **38**, 427 (2000)
4. H. W. Kroto, J. R. Heath, S. C. O'Brien, R. F. Curl, and R. E. Smalley, Nature **318**, 162 (1985)
5. W. Krätschmer, K. Fostiropoulos, and D. R. Huffman, Chem. Phys. Lett. **170**, 167 (1990)
6. "*Fullerenes, semiconductor surfaces, coherent phonon*s" edited by M. Cardona and G. Güntherodt , Springer, Berlin (2000)
7. R. H. Baughman, A. A. Zakhidov, and W. A. de Heer, Science **297**, 5582 (2002)
8. "*Carbon nanotubes : synthesis, structure, properties, and applications*" edited by M. S. Dresselhaus, G Dresselhaus, and P. Avouris, Springer, Berlin (2001)
9. G. von Helden, M.-T. Hsu, N. Gotts, and M. T. Bowers, J. Phys. Chem. **97**, 8182 (1993)
10. N. G. Gotts, G. von Helden, and M. T. Bowers, Int. J. Mass Spectrom. Ion Process **149/150**, 217 (1995)
11. R. E. Honig, J. Chem. Phys. **22**, 126 (1954)
12. J. Drowart, R. P. Burns, G. DeMaria, and M. G. Inghram, J. Chem. Phys. **31**, 1131 (1959)
13. P. D. Zavitsanos and G. A. Carlson, J. Chem. Phys. **59**, 2966 (1973)
14. J. M. L. Martin, J. P. François, and R. Gijbels, J. Chem. Phys. **95**, 9420 (1991)

15. J. M. L. Martin and P. R. Taylor, J. Chem. Phys. **102**, 8270 (1995)
16. "*Laser ablation : principles and applications*" edited by J. C. Miller, Springer, Berlin (1994)
17. "*Laser Ablation and Desorption*" edited by J. C. Miller and R. F. Haglund, Academic Press, San Diego (1998)
18. E. A. Rohlfing, J. Chem. Phys. **89**, 6103 (1988)
19. A. A. Puretzky, D. B. Geohegan, R. E. Haufler, R. L. Hettich, X.-Y. Zheng, and R. N. Compton, AIP Conf. Proc. **288**, 365 (1993)
20. K. Sasaki, T. Wakasaki, S. Matsui, and K. Kadota, J. App. Phys. **91**, 4033 (2002)
21. E. A. Rohlfing, D. M. Cox, and A. Kaldor, J. Chem. Phys. **81**, 3322 (1984)
22. Q. L. Zhang, S. C. O'Brien, J. R. Heath, R. F. Curl, H. W. Kroto, and R. E. Smalley, J. Phys. Chem. **90**, 525 (1986)
23. D. M. Cox, K. C. Reichmann, and A. Kaldor, J. Chem. Phys. **88**, 1588 (1988)
24. E. A. Rohlfing, J. Chem. Phys. **93**, 7851 (1990)
25. J. A. Zimmerman, J. R. Eyler, S. B. H. Bach, and S. W. McElvany, J. Chem. Phys. **94**, 3556 (1991)
26. S. B. H. Bach and J. R. Eyler, J. Chem. Phys. **92**, 358 (1990)
27. R. Ramanathan, J. A. Zimmerman, and J. R. Eyler, J. Chem. Phys. **98**, 7838 (1993)
28. J. F. Ward and G. H. C. New, Phys. Rev. **185**, 57 (1969)
29. A. H. Kung, J. F. Young, and S. E. Harris, Appl. Phys. Lett. **22**, 301 (1973)
30. K. Kaizu, K. Kohno, S. Suzuki, H. Shiromaru, T. Moriwaki, and Y. Achiba, J. Chem. Phys. **106**, 9954 (1997)
31. T. Wakabayashi, T. Momose, and T. Shida , J. Chem. Phys. **111**, 6260 (1999)

32. J. R. Heath, Q. Zhang, S. C. O'Brien, R. F. Curl, H. W. Kroto, and R. E. Smalley, J. Am. Chem. Soc. **109**, 359 (1987)
33. H. W. Kroto, J. R. Heath, S. C. O'Brien, R. F. Curl, and R. E. Smalley, Astrophys. J. **314**, 352 (1987)
34. M. Doverstål, B. Lindgren, U. Sassenberg, and H. Yu, Z. Phys. D **19**, 447 (1991)
35. R. P. Hallet, K. G. McKay, S. P. Balm, A. W. Allaf, H. W. Kroto, and A. J. Stace, Z. Phys. D **34**, 65 (1995)
36. P. Botschwina, Phys. Chem. Chem. Phys. **5**, 3337 (2003)
37. K. S. Pitzer, and E. Clementi, J. Am. Chem. Soc. **81**, 4477 (1959)
38. R. Hoffmann, Tetrahedron **22**, 521 (1966)
39. J. Hutter, H. P. Lüthi, and F. Diedrich, J. Am. Chem. Soc. **116**, 750 (1994)
40. K. Raghavachari and J. S. Binkley, J. Chem. Phys. **87**, 2191 (1987)
41. C. Liang and H. F. Schaefer III, J. Chem. Phys. **93**, 8844 (1990)
42. S. Yang, K. J. Taylor, M. J. Craycraft, J. Conceicao, C. L. Pettiette, O. Cheshnovsky, and R. E. Smalley, Chem. Phys. Lett. **144**, 431 (1988)
43. H. Handschuh, G. Ganteför, B. Kesseler, P. S. Bechthold, and W. Eberhardt, Phys. Rev. Lett. **74**, 1095 (1995)
44. J. D. Presilla-Márquez, J. A. Sheehy, J. D. Mills, P. G. Carrick, and C. W. Larson, Chem. Phys. Lett. **274**, 439 (1997)
45. S. L. Wang, C. M. L. Rittby, and W. R. M. Graham, J. Chem. Phys. **107**, 6032 (1997)
46. S. L. Wang, C. M. L. Rittby, and W. R. M. Graham, J. Chem. Phys. **107**, 7025 (1997)

47. J. D. Presilla-Márquez, J. Harper, J. A. Sheehy, P. G. Carrick, and C. W. Larson, Chem. Phys. Lett. **300**, 719 (1999)

48. T. Wakabayashi, T. Momose, T. Shida, H. Shiromaru, M. Ohara, and Y. Achiba, J. Chem. Phys. **107**, 1152 (1997)

Chapter 1

Preferential formation of neutral C_{10} upon laser vaporized graphite in He gas as studied by photoionization mass spectroscopy with 10.5 eV photons

1.1 Abstract

Neutral carbon clusters produced from laser-ablated graphite in a supersonic pulsed-helium expansion source were studied by time-of-flight (TOF) mass analysis using single-photon ionization with 10.5 eV photons. Varying the delay time of an ionization laser pulse relative to a vaporization pulse, we found that a signal of C_{10}, along with a weaker signal of C_{12}, was intensified almost exclusively to the other C_n signals with relatively long delay times of 80–250 μs. We observed two distinctly different TOFs for one and the same size, a short TOF at shorter delay times and a long TOF at longer delay times. We attribute the difference in TOF to the difference in initial velocity of the neutral cluster. We also performed the experiment within a high vacuum to find a similar difference in TOF for clusters of the same mass. The bimodal arrival-time distribution from the source to the ionization region indicates that the bunch of laser-ablated clusters separates into two bunches with different velocities. We

attribute this separation to the formation of a relatively dense boundary layer. During collisions behind the boundary, the relatively stable neutral C_{10}, probably of a monocyclic structure, is formed preferentially. This must be the origin of the selective detection of C_{10} at the longer delay times.

1.2 Introduction

Small carbon clusters, C_n (n=2–30), have not only attracted general attention as spectroscopic interests [1,2] but also as possible building units of fullerenes and nanotubes [3–5]. So far, pulsed-laser vaporization has been widely used for producing these clusters, and their growth, fragmentation, and isomerization processes have been studied extensively[6–14]. Recently, using high-speed imaging techniques, space–time evolution of laser-ablated plasma plumes has been studied and compared with the formation of fullerenes [15–17]. However, the relationship between the abundance of C_n clusters and the formation of fullerenes and nanotubes is still under debate. One of the difficulties in such investigations arises from the relatively high ionization potentials of neutral C_n clusters [18,19]. Mass spectroscopy with multiphoton ionization has been widely used to detect the carbon clusters because ofits high sensitivity. However, it was demonstrated that multiphoton ionization often leads to secondary fragmentation [20]. Thus, the distribution of size determined by the multiphoton ionization mass spectroscopy may vary greatly from the actual size distribution of the neutral clusters.

It has been shown that single-photon ionization must be more appropriate than multiphoton ionization to investigate the size distribution of neutral clusters. Recently, Achiba et al. have reported nascent mass distribution of laser vaporized neutral C_n

clusters of n≥6 in helium buffer gas using single-photon ionization mass spectroscopy [20]. They found that the distribution of neutral C_n in laser-ablated plasma was similar to that of anionic C_n^- produced simultaneously by the ablation laser pulse. For both the neutrals and the anions, signals of n=10 and of even-numbered larger sizes were pronounced. Wakabayashi et al. applied the same single-photon ionization technique to laser ablated graphite within a high vacuum to find a more distinct magic number behavior of C_{4n+2} (n=2–4) [21].

We performed herein the measurement of neutral mass distribution of laser-vaporized graphite in He buffer gas, extending the condition of Ref. 20 to various delay times of the ionization laser pulse relative to the vaporization pulse. The longer delay times studied here are comparable to those applied in a previous work in which the tandem irradiation of graphite with infrared (IR) and ultraviolet (UV) laser pulses under high vacuum yielded anionic C_{10}^- almost exclusively [22]. It was suggested that the selective anion was formed by the attachment of slow photoelectrons produced from the second UV pulse to neutral C_{10} formed from the preceding IR ablation pulse. The result of the present study gives the first clear evidence for such slow formation of neutral C_{10} in laser ablation processes.

1.3 Experiment

A rotating and translating graphite rod of natural isotopic abundance (1.1% ^{13}C and 98.9% ^{12}C) was vaporized in a narrow channel (2 mm in diameter and 12 mm long) of a metal block by moderately focused laser pulses from a Nd:YAG laser (Spectra Physics DCR-11, 532 nm, 7 ns duration) to form neutral C_n clusters along with cations

and anions. The clusters thus produced were expanded into a vacuum with a pulsed helium gas flow and lead to an ionization region composed of three disc electrodes having a central hole with a metal mesh. The distance from the vaporization source to the first electrode was 54 mm. The distances between the first and the second electrodes and the second and the last electrodes were 17 and 12 mm, respectively.

High voltage charges of direct current at +5.00 and +4.11 kV were applied to the first and the second electrodes, respectively, while the last one was grounded. The high voltage of the first electrode deflects the cations from the source. On the other hand, the anions accelerated to the first electrode, but they decelerated and scattered during traveling through the holes of the three disk electrodes. Thus, both the cations and the anions produced by the laser ablation processes do not appear in the mass spectrum.

The neutral C_n clusters that were not affected by these high voltages entered into the space between the first and the second electrodes with He buffer gases, where the clusters were photoionized by the second laser pulse of 10.5 eV photons. The distance from the vaporization source to the ionization region was 60 mm. The photoionized cations of C_n^+ accelerated by the electric fields of the three electrodes were drifted in a field free region of 40 cm, and then detected by a multi channel plates detector. All equipment, the source, the disk electrodes, and the detector, were set up coaxially. Owing to this coaxial configuration, we were able to separate not only the difference of masses, but also the difference of initial velocities of neutral clusters along the direction of gas expansion in the cluster source as a shift of mass peaks. (Details are given in the next section.)

Photons of 10.5 eV for the ionization were obtained by the ninth harmonic generation of Nd:YAG [23,24]. A pulsed laser beam of third harmonics of Nd:YAG (Continuum Powerlite 8010, 355 nm = 3.5 eV, 5 ns duration) was focused with a CaF_2 lens of 10 cm focal length in the middle of a gas cell containing xenon gas at 25 Torr to produce 118 nm (10.5 eV) photons [15]. The output beam of 10.5 eV photons from the cell was paralleled with an LiF lens and then separated from the beam of 355 nm with an LiF prism and an aperture of 6 mm in diameter. With this setup, only the 10.5 eV photons enter the ionization region to hit the neutral clusters.

The time-of-flight (TOF) spectrum of the ions was recorded on a digital oscilloscope (Tektronix TDS544A) with an acquisition of 1000 pulses. The system was operated at 10 Hz. The delay time of the ionization pulse relative to the vaporization pulse was varied from 10 to 1000 μs.

1.4 TOF Analysis

The TOF of a cluster with mass m and an initial velocity v_0 had been simulated numerically and it was found that it can be fitted well to the analytical expression

$$t = \alpha m^{1/2} - \beta m v_0 + t_0 \quad (1),$$

where α, β and t_0 are constants. The physical interpritation of this equation will be refered in chapter 3. The second term of the righthand side is typically on the order of 0.5% of the first term for C_{10} under the present experimental condition. The linearity to v_0 is held for the condition in which the ratio of acceleration voltages applied to the

first and second electrodes is tuned to give the sharpest TOF signal. The coefficient β in Eq. (1) is calculated to be 1.78×10^{-13} $amu^{-1}m^{-1}s^2$ for the present experimental setup, where m is given in an atomic mass unit. The shift in TOF corresponding to mass difference by one (Δm=+1) is obtained from Eq. (1) to be

$$\alpha[(m+1)^{1/2}-m^{1/2}]-\beta v_0 \quad \text{(isotopomeric shift)} \quad (2).$$

This isotopomeric shift becomes smaller as the value of m increases. On the other hand, the shift in TOF for clusters with the same mass but with different velocities is given by

$$-\beta m(v_0'-v_0) \quad \text{(velocity difference shift)} \quad (3).$$

This shift is proportional to both the velocity difference $\Delta v_0=v_0'-v_0$ and the mass m. The velocity difference shift becomes larger as the mass m increases, in contrast to the isotopomeric shift in Eq. (2). These relations in Eqs. (2) and (3) will be applied to the analysis of the splitting of mass peaks discussed in the subsequent section.

1.5 Results

1.5.1 Mass spectra in He buffer gas

Figure 1-1 shows TOF mass spectra of laser vaporized graphite in He buffer gas subsequently ionized with 10.5 eV photons. The numbers to the right of the spectra represent the delay times in μs of the ionization laser pulse to the preceding

vaporization pulse. The assignment n of C_n is indicated in the third panel from the bottom. The clusters larger than C_5 are detected in the mass spectra, since the ionization potentials of C_n for $n \geq 6$ are lower than 10.5 eV but those for $n \leq 5$ are higher than 10.5 eV [2,18,19]. In the third panel from the bottom (delay = 54 μs), mass peaks from n=6 to 18 are clearly seen with the intensity maximum for the C_{10} signal. The spectral distribution is essentially the same as that reported previously [20]. Sizable mass peaks are seen in the upper panels from 58 to 66 μs then fade away to 80 μs. Instead, a peak with slightly longer TOF values from the peak of C_{10} emerges between 70 and 80 μs. Another peak appears in these delay times near the peak of C_{12}. These new peaks are intensified throughout all the longer delay times studied exhibiting the intensity maximum at roughly 160 μs. At the delay time of 400 μs (uppermost of Fig. 1-1) one of the peaks is still discernible.

The peak at t = 5.7 μs appearing in longer delay times shifts by about ~30 ns from the peak of C_{10} observed in shorter delay times. One might consider that the former was due to hydrocarbon radical $C_{10}H$. However, we could deny this possibility because there was no additional source of hydrogen. Thus we must consider the possibility that the TOF can vary for one and the same mass, that is, the shift in TOF is due to the difference of initial velocity of the neutral cluster drifting in the ionization region. When the neutral cluster has, for example, a large velocity in the direction of the flight axis, the TOF of the corresponding cation is shortened accordingly as seen in Eq. (1). Employing the value β given in Sec. 4, the difference of 30 ns in TOF under the experimental condition corresponds to the velocity difference of $\Delta v_0 \sim 1400$ ms^{-1} [Eq. (3)], which is roughly equal to the difference calculated from the gas

dynamics (see section 6.1). Thus, we conclude that the delayed peak is also due to C_{10}^+. In other words, the velocity of C_{10} detected in shorter delay times is roughly 1400 ms^{-1} larger than the velocity of C_{10} in longer delay times.

Figure 1-2 depicts two distinctly different mass patterns for the "delayed" (longer delay times) and "prompt" (shorter delay times) clusters. The two spectra in Fig. 1-1, namely those of the delay times of 160 μs for (a) and of 58 μs for (b), are reproduced as a function of the unit of mass. The selective signal of C_{10} and C_{12} is noticeable in (a), while rather nonselective formation of various n of C_n in (b). Figure 1-3 shows the intensity profile as a function of the delay time for the "prompt" (closed circles) and "delayed" (open circles) signals of C_{10}. Note that the temporal intensity for the delayed signal is at most one-fourth of the maximum for the prompt signal. However, integrated intensity over the range of 70–400 μs is comparable to, or even higher than, the integrated intensity of the prompt signal in 40–80 μs.

1.5.2 Mass spectra within a high vacuum

In order to examine the effect of buffer gas upon the shift of TOF signals (70–80 μs in Fig. 1-1), we also re-examined our group's previous TOF mass spectroscopic experiments of laser ablated C_n within a high vacuum [21]. In the previous study, for which a rotating graphite pellet was set at the center of the first electrode and the flight tube was longer (~65 cm), laser ablated neutral C_n clusters were ionized with 10.5 eV photons 4 mm above the graphite target to obtain TOF mass spectra. All these procedures were performed within a high vacuum (2×10^{-8} Torr). Figure 1-4 shows mass spectra of laser-ablated C_n clusters in a high vacuum. Selected spectra are of the

delay times of (a) 40 μs and (b) 20 μs. A similar splitting of mass peaks, as those in Fig. 1-1 (70–80 μs), was also observed in a high vacuum.

In the upper panel spectrum (a), the splitting is clearly evinced by several mass peaks. Each delayed signal indicated by an open circle is visible in comparable intensity to its adjacent prompt signal indicated by a closed circle. The splitting for the signal of C_{10} is ~24 ns, while larger clusters exhibit larger splitting, namely ~33 ns for C_{14} and ~44 ns for C_{18} . The inset in Fig. 1-4 (a) shows a plot of these shifts as a function of the cluster size n of C_n. The linear dependence of the TOF shift as a function of the cluster size is in good agreement with the prediction from Eq. (3) (velocity difference shift). The linearity also indicates that velocity differences between the prompt and delayed clusters are the same for all C_n clusters wherein n=10 to 18. Thus we can naturally conclude that the delayed clusters must have a common velocity irrespective of their masses.

In the lower panel spectrum (b), a magic number behavior of C_{4n+2} (n=2–4) was clearly visible. A prominent peak of C_{10}, indicated by a closed circle, is accompanied by a smaller peak, indicated by a diamond. The latter peak is attributable to the isotopomer of $^{13}C^{12}C_9$. For C_{14} and C_{18}, accompanying peaks indicated by diamonds are also attributable to the isotopomers of $^{13}C^{12}C_{13}$ and $^{13}C^{12}C_{17}$. The inset in (b) shows the shift in TOF between adjacent peaks with a diamond and with a closed circle as a function of n of C_n. The dotted curve represents a simulated curve using Eq. (2) (isotopomeric shift). The agreement between the dotted curve and the observed shift shown in the inset of Fig. 1-4 (b) is good, which supports the assignment of the delayed peaks to the isotopomers, but not to the difference of initial velocity as in the delayed

peaks in Fig. 1-4 (a). The observed intensity ratios in Fig. 1-4 (b) are also in good agreement when calculated with the abundance ratio for the isotopomer of $^{13}C^{12}C_{n-1}$ relative to $^{12}C_n$.

1.6 Discussion

1.6.1 Separation of cluster bunches upon laser ablation

From the observed peak splitting, we infer that laser ablation ejectants separate into two bunches of different velocities. Such separation of laser ablation products was often confirmed experimentally (including laser ablation of graphite [15]), and theoretical characterizations of laser ablated plumes have been done [25]. It is not easy to translate the present experimental data into the gas dynamics of ablated plumes, because the instrumental setup of laser ablation cluster source used in present experiment was not optimum for the precise analysis of ablated plume dynamics. We tentatively propose, however, that the observed bunch separation was due to the formation of dense boundary layer consisting of emitted carbon species and buffer gas molecules in the plume. The formation of such boundary will split the clusters into two bunches. Clusters behind the boundary may be subjected to heavier collisions with other clusters and/or buffer gas cause rearrangement of cluster size and its structure.

The separated peaks for each C_n cluster were observed not only in helium buffer gas condition but also in high vacuum condition. The velocity of each bunch can be estimated roughly for the vacuum condition experiment. Since the distance from the graphite surface to the ionization region is 4 mm and the optimum delay for the

observation of the splitting is 40 μs, the velocity is estimated to be less than 100 ms^{-1}. In contrast, the other bunch of clusters, which is able to escape being trapped by collisions behind the boundary, has a larger velocity of >1300 ms^{-1}, since the maximum intensity of the prompt signal is observed within a delay time of a few μs (cf. Fig. 1-1 in Ref. 21). The difference in velocity deduced here agrees with the difference estimated from the splitting of mass peaks in Fig. 1-4 (a) and Fig. 1-1. But it cannot necessarily be concluded that the separations observed in both the buffer gas conditions and vacuum condition were based on the same cause, because many precedent researches for laser ablation process have shown that the dynamics of laser ablated plumes were much affected by existence of ambient gas. In laser ablation process of graphite under high vacuum, similar splittings of TOF mass peaks for C_n^+ ions directly produced by ablation were observed by Choi et al. [26] and they concluded that the separation of ejecta is due to the formation of Knudsen layer [25,27].

Further research for laser-induced gas dynamics based on finer experiments is performed in Chapter 3.

1.6.2. Preferential formation mechanism of C_{10}

Secondary reactions behind a boundary should be responsible for the selective signal of C_{10} [Fig. 1-2 (a)]. Multiple collisions are major processes in such gas mixtures. In the case of faster growth and slower cooling, the extra energy of newly formed C−C bonds is transferred to an internal energy to heat up the cluster, which leads to the rearrangement or decomposition of C−C bonding to produce more stable fragments. Energetic collisions during the formation of a dense layer may also heat up

the cluster to dissociate it into smaller clusters. Such time-consuming fragmentation of larger clusters is conceivable for the mechanism of preferential formation of C_{10}.

Bowers and his colleagues have reported preferential loss of neutral C_{10} upon the metastable fragmentation of laser vaporized cluster cations of C_n^+ (n=24–29) [10]. Bowers et al. [11] and Jarrold et al. [12,13] have reported preferential loss of C_{4n+2} upon the collision-induced dissociation of C_n^+, attributing such to monocyclicity. We deduce that for neutral clusters as well such preferential fragmentation channels exist to explain the abundance of C_{10}. Therefore, we propose that the neutral C_{10} detected at the longer delay times has a monocyclic form.

Monocyclic C_n clusters have been studied as factors that challenge theoretical and experimental issues [28–33]. Earlier theoretical studies have predicted stability of even-numbered monocycles of C_{2n} [28,29], and aromatic stabilization for the carbon ring size of $4n$+2 [30]. Recently, the distortion of larger carbon rings has been discussed extensively [31–33]. Smalley et al. suggested that such monocyclicity resulted from laser-vaporized carbon clusters [34]. By using anion photoelectron spectroscopy, they found a different series of C_n clusters with relatively low electron affinities for n=10–29 which was attributable to monocyclic clusters. Molecular structures of C_n^- have also been investigated by ion mobility measurement [9,14]. All of these studies indicate that the neutral C_{10} cluster is the smallest monocyclic ring among the C_n clusters in the gas phase [1].

It has been suggested that the monocyclic C_{10} cluster forms preferentially under the present experimental condition in He buffer gas. It is worthwhile to note that the smallest linear chain molecule of C_3 predominates carbon vapor molecules within a

high vacuum [1,2,28], while the smallest closed-cage molecule of C_{60} predominates under relatively high-pressure conditions [3,4,7,35]. Analogously to the case of C_{60}, the smallest monocyclic C_{10}, once formed as the stable fragment, can survive against further collisions with other clusters in the buffer gas [36]. The selective formation of neutral C_{10} found in the present work may be applicable to the spectroscopy of monocyclic carbon ring molecules and open a way to the synthesis of novel functionality materials consisting of sp carbon atoms.

References

1. Van Orden and R. J. Saykally, Chem. Rev. **98**, 2313 (1998).
2. W. Weltner, Jr. and R. J. Van Zee, Chem. Rev. **89**, 1713 (1989).
3. H. W. Kroto, J. R. Heath, S. C. O'Brien, R. F. Curl, and R. E. Smalley, Nature **318**, 162 (1990).
4. W. Krätschmer, L. D. Lamb, K. Fostiropoulos, and D. R. Huffman, Nature **347**, 350 (1990).
5. S. Iijima, Nature **354**, 56 (1991).
6. E. A. Rohlfing, D. M. Cox, and A. Kaldor, J. Chem. Phys. **81**, 3322 (1984).
7. D. M. Cox, K. C. Reichmann, and A. Kaldor, J. Chem. Phys. **88**, 1588 (1988).
8. T. Moriwaki, K. Kobayashi, M. Osaka, M. Ohara, H. Shiromaru, and Y. Achiba, J. Chem. Phys. **107**, 8927 (1997).
9. N. G. Gotts, G. Von Helden, and M. T. Bowers, Int. J. Mass Spectrom. Ion Processes **149/150**, 217 (1995).
10. P. P. Radi, T. L. Bunn, P. R. Kemper, M. E. Molchan, and M. T. Bowers, J. Chem. Phys. **88**, 2809 (1988).
11. G. von Helden, N. G. Gotts, and M. T. Bowers, J. Am. Chem. Soc. **115**, 4363 (1993).
12. J. Hunter, J. Fye, and M. F. Jarrold, J. Phys. Chem. **97**, 3460 (1993).
13. J. M. Hunter, J. L. Fye, and M. F. Jarrold, J. Chem. Phys. **99**, 1785 (1993).
14. Ph. Dugourd, R. R. Hudings, J. M. Tenenbaum, and M. F. Jarrold, Phys. Rev. Lett. **80**, 4197 (1998).

15. A. A. Puretzky, D. B. Geohegan, R. E. Haufler, R. L. Hettich, X.-Y. Zheng, and R. N. Compton, AIP Conf. Proc. **288**, 365 (1994).
16. T. Ishigaki, S. Suzuki, H. Kataura, W. Krätschmer, and Y. Achiba, Appl. Phys. A **70**, 121 (2000).
17. D. Kasuya, F. Kokai, K. Takahashi, M. Yudasaka, and S. Iijima, Chem. Phys. Lett. **337**, 25 (2001).
18. R. Ramanathan, J. A. Zimmerman, and J. R. Eyler, J. Chem. Phys. **98**, 7838 (1993).
19. S. B. H. Bach and J. R. Eyler, J. Chem. Phys. **92**, 358 (1990).
20. K. Kaizu, K. Kohno, S. Suzuki, H. Shiromaru, T. Moriwaki, and Y. Achiba, J. Chem. Phys. **106**, 9954 (1997).
21. T. Wakabayashi, T. Momose, and T. Shida, J. Chem. Phys. **111**, 6260 (1999).
22. T. Wakabayashi, T. Momose, T. Shida, H. Shiromaru, M. Ohara, and Y. Achiba, J. Chem. Phys. **107**, 1152 (1997).
23. A. H. Kung, J. F. Young, and S. E. Harris, Appl. Phys. Lett. **22**, 301 (1973).
24. J. F. Ward and G. H. C. New, Phys. Rev. **185**, 57 (1969).
25. for example, see R. Kelly, A. Miotello, A. Mele, and A. G. Guidoni, in "*Laser Ablation and Desorption*", edited by J. C. Miller and R. F. Haglund (Academic Press, San Diego, 1998), p.225.
26. Y.-K. Choi, H.-S. Im, K.-W. Jung, Int. J. Mass Spectrom. **189**, 115 (1999)
27. T. Ytrehus, in "*Rarefied Gas Dynamics*", edited by J. L. Potter (AIAA, New York, 1977), p.1197.
28. K. S. Pitzer and E. Clementi, J. Am. Chem. Soc. **81**, 4477 (1959).
29. K. Raghavachari and J. S. Binkley, J. Chem. Phys. **87**, 2191 (1987).

30. R. Hoffmann, Tetrahedron **22**, 521 (1966).

31. M. Saito and Y. Okamoto, Phys. Rev. B **60**, 8939 (1999).

32. E. J. Bylaska, R. Kawai, and J. H. Weare, J. Chem. Phys. **113**, 6096 (2000).

33. T. Torelli and L. Mitas, Phys. Rev. Lett. **85**, 1702 (2000).

34. S. Yang, K. J. Taylor, M. J. Craycraft, J. Conceicao, C. L. Pettiette, O. Cheshnovsky, and R. E. Smalley, Chem. Phys. Lett. **144**, 431 (1988).

35. T. Wakabayashi, D. Kasuya, H. Shiromaru, S. Suzuki, K. Kikuchi, and Y. Achiba, Z. Phys. D **40**, 414 (1997).

36. R. F. Curl and R. E. Smalley, Sci. Am. **265**, 54 (1991).

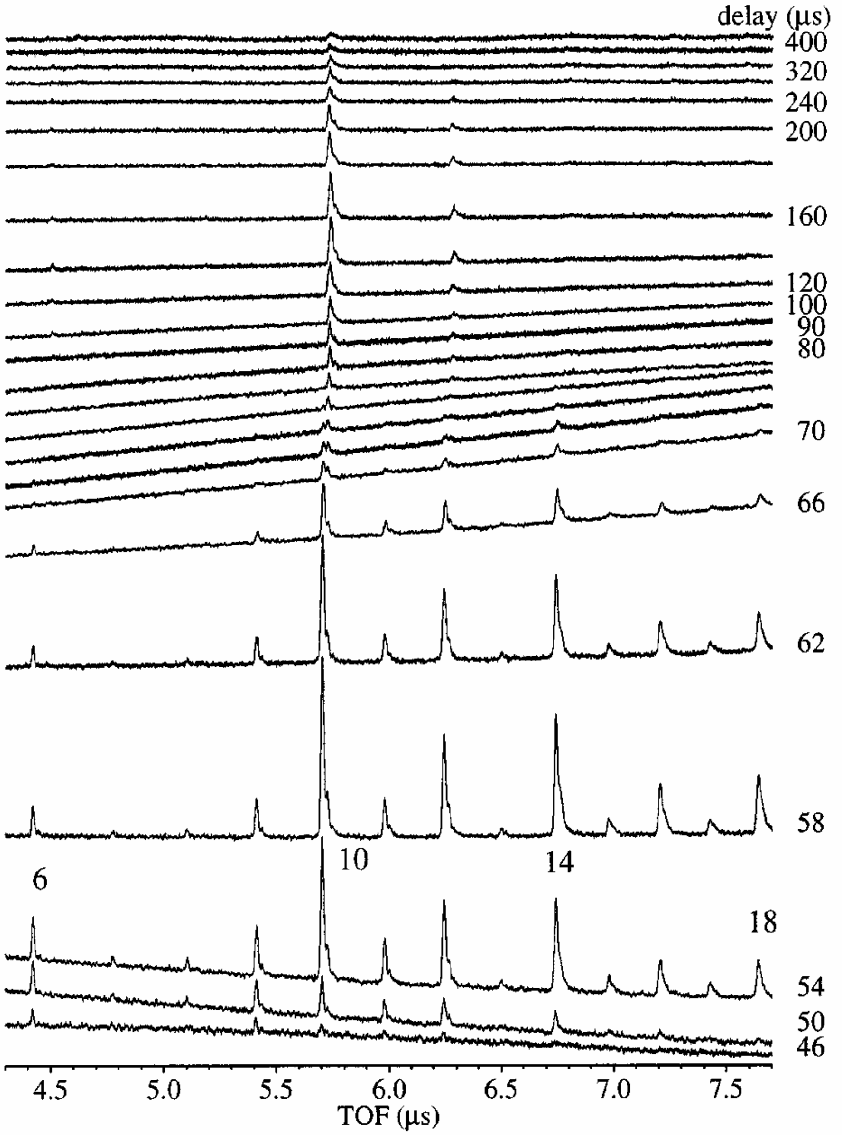

Fig. 1-1 TOF mass spectra of laser vaporized neutral C_n clusters in He buffer gas photoionized with 10.5 eV photons. The numbers to the right represent the delay times in μs of the ionization laser pulse relative to the preceding vaporization pulse. The cluster size n of C_n is indicated in the third panel from the bottom.

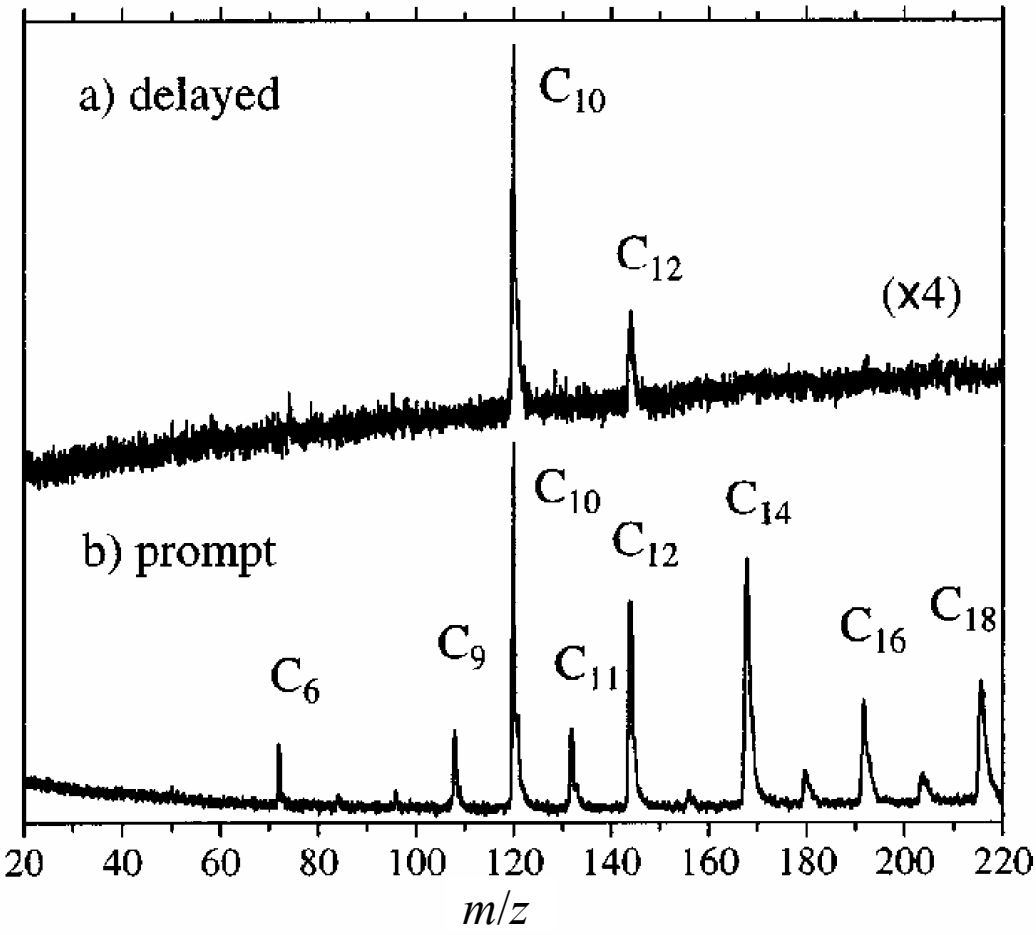

Fig. 1-2 Two distinctly different mass patterns of the (a) "delayed" and (b) "prompt" C_n clusters. The two spectra in Fig. 1-1, namely of (a) 160 μs and of (b) 58 μs, are reproduced as a function of the mass unit. For the intensity normalization, the upper panel spectrum (a) is multiplied by a factor of 4.

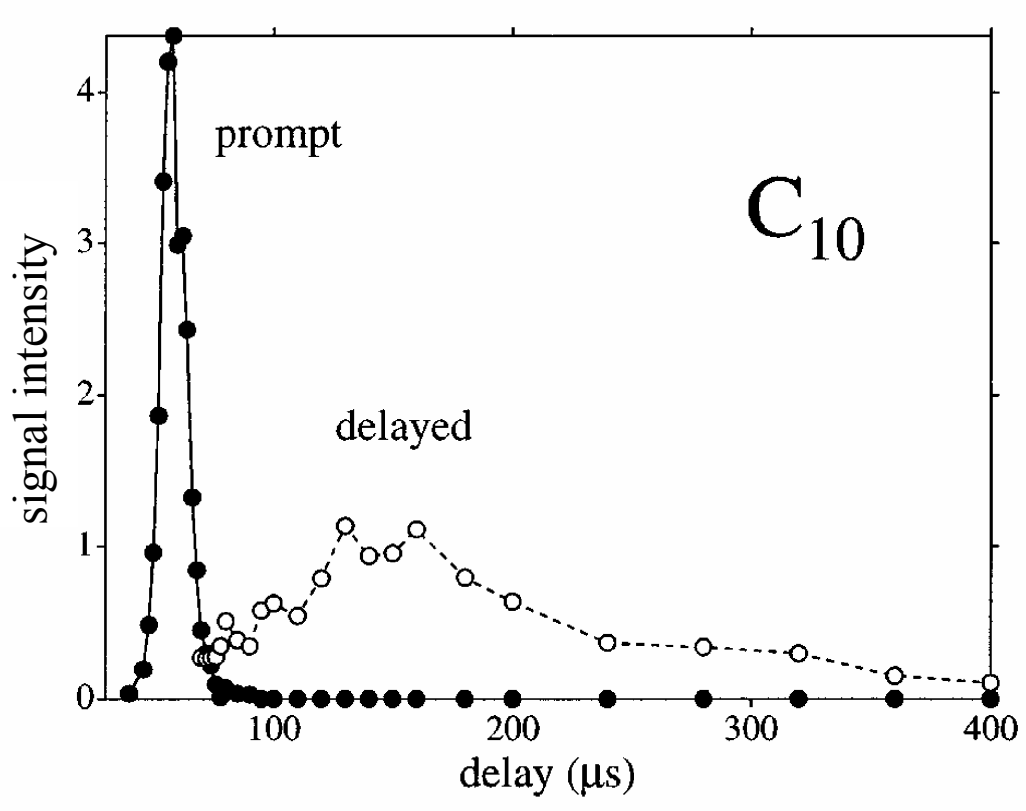

Fig. 1-3 The intensity profile of the "prompt" (closed circles) and "delayed" (open circles) signals of C_{10} in He gas as a function of the delay time.

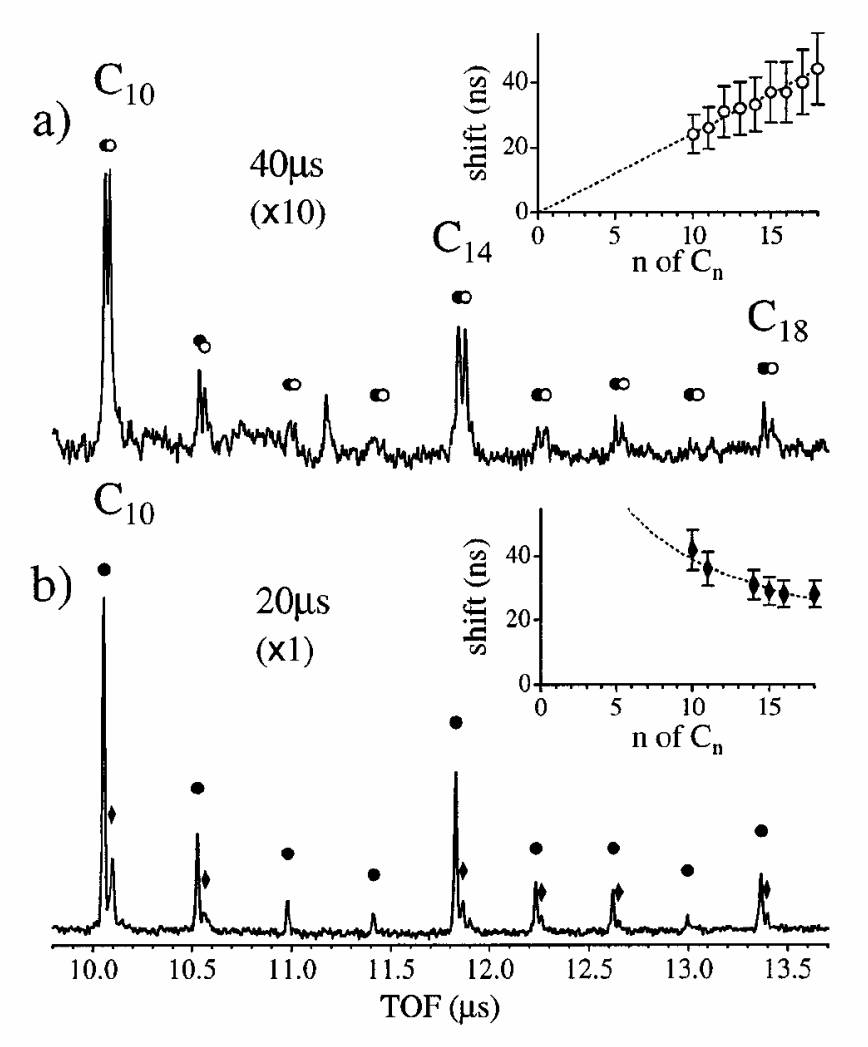

Fig. 1-4 The TOF mass spectra of laser-ablated graphite within a high vacuum subsequently photoionized with 10.5 eV photons. The spectra correspond to the delay times of (a) 40 μs and (b) 20 μs, displaying the prompt (closed circles) and delayed (open circles) signals. Peaks with diamonds are of the isotopomer, namely $^{13}C^{12}C_{n-1}$ of $^{12}C_n$. The insets show the cluster size dependence of the splitting in TOF for mass peaks in (a) and (b). For details, see text (section 5.2).

Chapter 2

A mass spectroscopic study of laser vaporized graphite in H_2 and D_2 gases: The stability of $C_{2n}H_2$ (n=2–5) and C_{10}

2.1 Abstract

Carbon clusters, hydrocarbon molecules and radicals produced by laser vaporization of graphite in a hydrogen (H_2 or D_2) gas expansion source were studied using 10.5 eV one-photon ionization followed by time-of-flight mass spectroscopy. By changing the delay time of the ionization pulse relative to the vaporization pulse, we found two distinctly different mass patterns: rather non-selective signals of C_n (n=6–20) and C_nH_m (n=3–20 and m=1–4) at shorter delay times, while selective signals of $C_{2n}H_2$ (n=2–5) and C_{10} at longer delay times. The selective formation of the carbon cluster and hydrocarbon molecules at longer delay times is attributed to the relatively inert nature of polyynes $H(-C\equiv C-)_nH$ (n=2–5) and monocyclic C_{10}. The formation mechanism of these hydrocarbons and carbon clusters by laser ablation under hydrogen gas is discussed.

2.2 Introduction

Carbon clusters and their hydrogenated derivatives have been studied in relation to interstellar chemistry, combustion chemistry, and material sciences. Reactivity of linear carbon clusters has been studied employing the laser ablation of graphite under the presence of various gases such as H_2 [1–5], D_2 [4], H_2O [1,2], D_2O [1], N_2 [1,2], CH_3CN [1,2], NH_3 [1,2], NO [6], and SO_2 [6]. It was found that polyynes $HC_{2n}H$ were formed abundantly in H_2 gas [1–5], and also cyanopolyynes $HC_{2n+1}N$ were abundant in CH_3CN and NH_3 gases [1]. These molecules were supposed to form as a result of the termination of reactive ends of linear clusters C_n by an H or N atom [1,2]. The stability of $HC_{2n+1}N$ accounts for the rich abundance of cyanopolyynes in interstellar space [7–11].

Recently, longer polyynes $HC_{2n}H$ (n=8–13) in the gas phase have been identified by Maier's group using resonant two-color two-photon resonance ionization spectroscopy [12]. Tsuji et al. produced polyynes $HC_{2n}H$ (n=4–8) through the laser ablation of graphite particles in solution [13]. Hirsch produced dicyanopolyynes $NC_{2n}N$ (n=4–9) by the arc discharge of graphite rods in the presence of dicyan gas [14]. Cataldo produced the series of polyynes $HC_{2n}H$ (n=2–9) and their derivatives by a submerged electric arc in organic solvents [15,16]. In the latter three experiments, the products were separated chromatographically and identified by electronic absorption spectra in solution [13,14,15,16].

Mass spectroscopy is a powerful technique for the detection of large carbon clusters, C_n (n≥4), since most of the clusters are difficult to detect optically in the gas phase. In most mass spectroscopic studies of carbon clusters so far reported, the ionization was done using photons emitted directly from commercially available lasers

such as ArF lasers (6.42 eV) [17]. Since the photon energy is lower than the ionization potential (IP) of most clusters C_n ($n \leq 80$), multi-photon ionization (MPI) is necessary to ionize the clusters [18–20]. However, the MPI may cause serious fragmentation of precursor clusters, so that the mass spectrum obtained by the MPI does not reflect the nascent mass distribution of the neutral clusters before the ionization.

In order to obtain information on mass distribution of the neutral clusters, it is desirable to ionize by a single-photon rather than by multi-photons in order to avoid serious fragmentation. Fullerenes such as C_{60} (E_i = 7.6 eV) have relatively small IP, and can be ionized by single-photon ionization using photons from F_2 lasers at 7.89 eV [3,5,6]. Recently, one-photon ionization of carbon clusters C_n down to n=6 was achieved by using 10.5 eV photons, which is the ninth harmonics of the fundamental radiation of Nd:YAG lasers [21–23]. We have studied carbon clusters produced by the laser ablation of graphite using one-photon ionization with the 10.5 eV photons, and found a condition for the preferential formation of neutral C_{10} clusters [23] and concluded that the preferential formation of C_{10} is a result of the formation of a dense boundary layer in the laser ablation process. Very recently, a similar laser-induced dence layer was intentionally applied to a size control of silicon clusters [24].

In this chapter, we have studied the mass spectra of carbon clusters and related hydrocarbon molecules produced by laser vaporization of graphite under the presence of H_2 or D_2 buffer gas using the 10.5 eV one-photon ionization in order to study the stability and formation mechanism of laser ablated carbon clusters. By changing the delay times of the ionization laser pulse relative to the vaporization laser pulse, we found a condition in which the highly unsaturated dihydrides C_4H_2, C_6H_2, C_8H_2, and

$C_{10}H_2$ were preferentially formed together with the carbon cluster C_{10}.

2.3 Experiments

2.3.1 Experimental setup

Figure 2-1 shows a schematic view of the apparatus and the time sequence for the measurements. The setup is essentially the same as that reported in Ref. 23 except for the use of H_2 or D_2 as a buffer gas. A graphite rod (^{12}C:^{13}C = 98.9:1.1) of 1 cm in diameter was ablated by an intense laser beam obtained by focusing the fundamental radiation of a Q-switched Nd:YAG laser (Spectra Physics DCR-11, 1064 nm, 7 ns duration). The diameter of the laser spot was ~1 mm on the target. The ablation was done under the presence of H_2 (99.99 %) or D_2 (99.9 %). The hydrogen gas was introduced by a pulsed valve (Parker-Hannifin General Valve 9–279–900). The stagnation pressure behind the pulsed valve was set at 3–5 atm. The vapor phase products were then carried by the hydrogen gas flow through a narrow channel of 2 mm in diameter and a length of 12 mm before expanding them into the vacuum. At 48 mm downstream of the exit of the channel, the products were ionized by a vacuum-ultraviolet (VUV) photon at 10.5 eV.

The VUV laser pulses were obtained by generating the third harmonics of 355 nm photons in Xe gas [22,23]. The third harmonics of an Nd:YAG laser (Continuum Powerlite 8010, 355 nm = 3.5 eV, 5 ns duration) was focused by a CaF_2 lens (f = 10 cm) in the middle of a gas cell (20 cm long) filled with ~25 Torr of Xe to generate photons at 118 nm (= 10.5 eV). The 10.5 eV radiation thus generated was made parallel by a LiF lens (f = 10 cm), separated from the 355 nm radiation by a LiF prism, and introduced

into the ionization region through an aperture of 6 mm in diameter.

The cations ionized by the VUV photons were accelerated by static electric fields (+5.00 kV and +4.09 kV) toward the detector (Galileo 6205 chevron-stacked multi channel plate) to obtain mass spectra. A digitizing oscilloscope (Tektronix TDS544A) was used to record the mass spectra with an acquisition of 1000 pulses. The system was synchronized by a delay generator (Stanford Research Systems DG535) at the repetition rate of 10 Hz. The delay time of the ionization laser pulse relative to the vaporization pulse was changed between 20 and 1000 μs.

2.3.2 IP of carbon clusters, hydrocarbons and radicals

Under our experimental condition, neutral species having lower IP than the photon energy of 10.5 eV were ionized and therefore able to detect by the mass spectroscopy. Figure 2-2 depicts the IP of carbon clusters C_n as a function of their masses per charge number. The horizontal dotted line corresponds to the energy of a 10.5 eV photon. The IP of bared carbon clusters C_n ranges from 6 to 13 eV, which were measured by the charge transfer reaction between C_n^+ and various molecules with a known IP [18–20]. The IP of C_2 was refined recently using charge-inversion, energy-loss spectroscopy [25]. The IP of a carbon atom was determined by VUV spectroscopy [26]. From Fig. 2-2 it is seen that only the clusters larger than C_5 can be ionized by one-photon at 10.5 eV.

The IP of some unbranched hydrocarbon molecules C_nH_m are also shown in Fig. 2-2 [27]. In general, the IP of the hydrocarbon molecules tends to decrease as the number of carbon atom (n) increases. Hydrocarbon molecules with an even number of electrons (the open triangles in Fig. 2-2) have a higher IP than radicals with an odd

number of electrons (symbolized by closed triangles). Most of them can be ionized by a single-photon at 10.5 eV. Polyynes $HC_{2n}H$ indicated by diamonds in Fig. 2-2 have a lower IP than 10.5 eV, except for that of C_2H_2 [28,29]. Saturated *n*-alkanes C_nH_{2n+2} (n=1–5) (closed circles) [28,30,31], methylidine CH [32], ethynyl C_2H [33], and ethylene C_2H_4 [28] cannot be ionized by a 10.5 eV photon as shown in Fig. 2-2.

2.4 Results and discussion

2.4.1 VUV photoionization mass spectra in H_2

Figure 2-3 shows the time-of-flight (TOF) mass spectra of the products obtained by laser vaporization of graphite under the presence of H_2 gas subsequently ionized with 10.5 eV photons. The spectra taken at different delay times of the ionization laser pulse relative to the vaporization pulse are shown for comparison. The numbers shown at the right of each spectrum represent the delay times in μs.

In the bottom trace (delay time 36 μs), mass peaks corresponding to C_nH_m (n≥3, m=0–4) are clearly seen. For odd n (n≥7), a smooth distribution of intensity of mass signals for m=0–4 was observed. The peaks of C_3 and C_5 were missing because of their larger IP than 10.5 eV [18]. The intense peak of C_3H indicates that the IP of C_3H is lower than 10.5 eV. For even n (n≥6), the signal of dihydrides C_nH_2 was the strongest among those of the same n, except for n=10 and 14, for which the signals of bared clusters C_{10} and C_{14} were the strongest. For n=4, only a peak of C_4H_2 was observed. The C_4 cluster may exist, but was not able to detect because of its larger IP than 10.5 eV [18].

The fact that the number of hydrogen atoms m in any detected hydrocarbon C_nH_m

is at most m=4 indicates that highly unsaturated carbon chain molecules were formed by the ablation. As for dihydrides C_nH_2, the alterations in intensity with respect to the carbon number n being odd or even were observed more clearly in the present experiment than in previous works [1–5].

Other traces in Fig. 2-3 show spectra at longer delay times up to 90 μs. The intensity of mass peaks decreased gradually as the delay time increased up to 40 μs, but increased again at 42 and 58 μs delay times. At 90 μs delay time, a distinctly different mass pattern compared with that at shorter delay times was observed. The peaks observed at 90 μs delay time can be assigned to C_4H_2, C_6H_2, C_8H_2, and C_{10}.

It is noted that peaks in the spectrum at 42 μs delay time shifted slightly from those at 40 μs delay time as indicated by dotted lines between the spectra from 38 μs through 58 μs delay. The shift of TOF peak of C_{10} (~33 ns for m/z=120) was larger than the shift of C_4H_2 (~15 ns for m/z=50). The shift in TOF is associated with the difference in the initial velocity of neutral clusters in the ionization region. In a previous chapter, we have discussed that the difference in the velocity is attributed to the separation of the expanding plasma plume by forming a dense boundary layer [23]. The separated two bunches of clusters have different velocities. Clusters traveling in front of the boundary have faster velocity, while those behind the boundary have slower velocity. Therefore, the mass signals observed at shorter delay times are attributed to the clusters in front of the boundary, while those observed at longer delay times are attributed to the clusters behind the boundary. The shift of mass peaks seen in Fig. 2-3 is due to this separation. Clusters behind the boundary are subjected to heavy collisions with other clusters, hydrocarbons, and radicals as well as with hydrogen

atoms and molecules. As a result, the species detected at longer delay times must be molecules that are more stable against the collisions.

2.4.2 Fast and slow components

Figure 2-4 plots the intensity of the mass signal as a function of the delay time for (a) C_6, (b) C_6H_2, and (c) C_{10}. A bimodal distribution is clearly seen for C_6H_2 in Panel (b). The fast component detected at shorter delay times (closed circles) showed the maximum at ~36 μs, while the slow component at longer delay times (open circles) showed the maximum at ~90 μs. The fast and slow components correspond, respectively, to clusters in front of the boundary and to those behind the boundary as discussed above.

In Panel (c), a slight amount of the slow component of C_{10} was seen, but the amount was not as much as that observed in He buffer gas [23]. In hydrogen buffer gas, a part of C_{10} clusters may react with hydrogen and/or hydrocarbons and thereby reduce the abundance of clusters. No trace of the slow component was observed for C_n and C_nH_m other than C_{10} (and a pretty little for C_{12}) and $C_{2n}H_2$ (n=2-4) as shown for C_6 in Panel (a), as an example of this.

As shown in figure 2-5, these dihydrides $C_{2n}H_2$ had kept or slightly strengthened their signal intensity in the delay time longer than 200 μs (Fig. 2-5 (a) for C_8H_2), unlike the carbon clusters observed in delayed component (Fig. 2-5 (b) for C_{10}). This result suggests the different formation mechanism between $C_{2n}H_2$ and C_{10} in the delayed components, or there is another process to produce only the dihydrides. Detailed consideration about the dissimilar between $C_{2n}H_2$ and C_{10} is performed in the next

chapter.

2.4.3 Dependence of vaporization laser power in D_2 buffer gas

In order to obtain information on the formation mechanism of hydrocarbons observed in the mass signals, we have investigated the dependence of mass patterns on the power of the vaporization laser pulses. In this experiment D_2 was used as a buffer gas, because mass peaks of monodeuteride C_nD can be clearly distinguished from the peak of the isotopomer $^{13}C^{12}C_{n-1}$. The experimental conditions were the same as those described in Sec. 2 except for the power of the vaporization pulse.

Figure 2-6 shows mass spectra obtained with various powers of the vaporization laser pulses. Panel (a) shows mass spectra of the fast component (46 μs delay time), and Panel (b) shows those of the slow component (146 μs delay time). From the bottom to the top of each panel, the laser power corresponds to 20, 26, and 32 mJ/pulse, respectively.

With the lower intensity of the vaporization pulses (20 mJ/pulse), peaks of bared clusters such as C_{10}, C_{12}, and C_{14} were observed strongly in the fast component. As the laser intensity increased (26 and 32 mJ/pulse), the intensity of peaks of hydrocarbons increased. Under vaporization pulses of high intensity, it is expected that hydrogen molecules are decomposed thermally into hydrogen atoms [34], they will be indispensable to form the hydrocarbons.

It should be noted that the intensity of peaks of bared carbon clusters C_n in the fast component kept roughly constant irrespective of the power of the vaporization laser pulses, while the intensity of peaks of hydrocarbons increased monotonically as the

power of the vaporization laser pulses increased. The different behavior between the carbon clusters and hydrocarbon molecules with respect to the vaporization laser power suggests that the small carbon clusters observed in Fig. 2-6 might not be the precursors of hydrocarbon molecules. It is assumable that the increase of ablation laser power results in the generation of more reactive isomers and/or excited states of C_n, and they are the precursors of the dihydrides but not the carriers of observed carbon cluster signals.

The dominance of $C_{2n}D_2$s in proportion to other hydrocarbon species allows to conjecture the other process of their selective formation. It is known that large carbon clusters or carbon grains are produced in abundance with intense vaporization laser pulses [35]. Devienne and Teisseire showed that graphite bombardment by high-energy neutrals can produce long carbon chain species [36]. Therefore, laser ablated large carbon clusters and/or carbon particles may be possible to produce observed dihydrides by the reaction with hydrogen atoms. As Kroto et al. felt [1,2], the laser ablation experiments may demonstrate the simple way of long polyynes formation in the interstellar regions.

As for the slow component, peaks of $C_{2n}D_2$ (n=2–5) were observed exclusively together with the peak of C_{10} with any vaporization power. The intensity of peaks of $C_{2n}D_2$ (n=2–5) increased as the power increased**,** as in the case of the fast component. The mechanism of the exclusive existence of C_{10} and $C_{2n}D_2$ (n=2–5) is discussed below.

2.4.4 Fragmentation and survival

The selective signals of C_{10} and $C_{2n}D_2$ (n=2–5) in the slow component as shown in

Panel (b) of Fig. 2-6 are noteworthy. Two origins are conceivable for the exclusive existence of these molecules in the slow component: one being selective formation and the other being survival.

Clusters and hydrocarbons in the slow component are subjected to multiple collisions with other clusters, hydrocarbons, and radicals, as well as with hydrogen atoms and molecules. During these collisions, carbon chain molecules may polymerize into larger clusters, which could not be observed under the present experimental conditions. It has been discussed that stable neutral fragments, i.e. monocyclic C_{10} carbon clusters**,** may be ejected preferentially from the larger carbon clusters [37]. Part of the C_{10} detected in the slow component would originate in the fragmentation from the larger carbon clusters.

Moreover, molecules observed behind the boundary would survive from heavy collisions, and thus chemically inert molecules could only survive there. Polyynes are rather stable against the collisions, and thus they were observed selectively in the slow component. The survival of the C_{10} implies that it has a monocyclic form, since the linear C_{10} may be not stable against collisions with H or H_2. In the slow component, the monocyclic C_{10} will fragment selectively and/or survive.

2.5 Conclusion

In this chapter, the origin of the carbon clusters and related hydrocarbon molecules produced by laser vaporization of graphite in a hydrogen (H_2 or D_2) ambient gas was discussed. The comparatively larger increase of $C_{2n}D_2$ signal than other hydrocarbon species upon the vaporization laser intensification brings a supposition that their

selective formation process exists e.g. carbon species bombardment by hydrogen atoms. The selective formation of C_{10} observed behind the boundary is attributable to the fragmentation of larger carbon clusters and/or to survival from heavy collisions. The survival of $C_{2n}H_2$ (n=2–5) is a result of the chemically inert nature of polyynes, and the survival of C_{10} indicates its monocyclicity. Detailed discussion on the laser ablation process will be discussed in next chapter [38].

References

1. J.R. Heath, Q. Zhang, S.C. O'Brien, R.F. Curl, and H.W. Kroto, R.E. Smalley, J. Am. Chem. Soc. **109**, 359 (1987).
2. H. W. Kroto, J.R. Heath, S.C. O'Brien, R.F. Curl, and R.E. Smalley, Astrophys. J. **314**, 352 (1987).
3. E.A. Rohlfing, J. Chem. Phys. **93**, 7851 (1990).
4. M. Doverstål, B. Lindgren, and U. Sassenberg, H. Yu, Z. Phys. D **19**, 447 (1991).
5. R.P. Hallet, K.G. McKay, S.P. Balm, A.W. Allaf, H.W. Kroto, and A.J. Stace, Z. Phys. D **34**, 65 (1995).
6. Q.L. Zhang, S.C. O'Brien, J.R. Heath, R.F. Curl, H.W. Kroto, and R.E. Smalley, J. Phys. Chem. **90**, 525 (1986).
7. B.E. Turner, Astrophys. J. **163**, L133 (1971).
8. L.W. Avery, N.W. Broten, J.M. MacLeod, T. Oka, and H.W. Kroto, Astrophys. J. **205**, L173 (1976).
9. H.W. Kroto, C. Kirby, D.R.M. Walton, L.W. Avery, N.W. Broten, J.M. MacLeod, and T. Oka, Astrophys. J. **219**, L133 (1978).
10. N. W. Broten, T. Oka, L.W. Avery, J.M. MacLeod, and H.W. Kroto, Astrophys. J. **233**, L105 (1978) L105.
11. M.B. Bell, P.A. Feldman, S. Kwok, and H.E. Matthews, Nature **295**, 389 (1982).
12. T. Pino, H. Ding, F. Güthe, and J.P. Maier, J. Chem. Phys. **114**, 2208 (2001).
13. M. Tsuji, T. Tsuji, S. Kuboyama, S.-H. Yoon, Y. Korai, T. Tsujimoto, K. Kubo, A. Mori, and I. Mochida, Chem. Phys. Lett. **355**, 101 (2002).

14. A. Hirsch, Habilitationsschrift der Eberhard-Karls-Universität Tübingen (1994).
15. F. Cataldo, Carbon **41**, 2653 (2003).
16. F. Cataldo, Carbon **42**, 129 (2004).
17. E.A. Rohlfing, D.M. Cox, and A. Kaldor, J. Chem. Phys. **81**, 3322 (1984).
18. R. Ramanathan and J.A. Zimmerman, J.R. Eyler, J. Chem. Phys. **98**, 7838 (1993).
19. S.B. H. Bach and J.R. Eyler, J. Chem. Phys. **92**, 358 (1990).
20. J.A. Zimmerman, J.R. Eyler, B.H. Bach, and S.W. McElvany, J. Chem. Phys. **94**, 3556 (1991).
21. K. Kaizu, K. Kohno, S. Suzuki, H. Shiromaru, T. Moriwaki, and Y. Achiba, J. Chem. Phys. **106**, 9954 (1997).
22. T. Wakabayashi, T. Momose, and T. Shida, J. Chem. Phys. **111**, 6260 (1999).
23. Y. Kato, T. Wakabayashi, and T. Momose, J. Chem. Phys. **118**, 5390 (2003).
24. Y. Iwata, M. Kishida, M. Muto, S. Yu, T. Sawada, A. Fukuda, T. Takiya, A. Komura, and K. Nakajima, Chem. Phys. Lett. **358**, 36 (2002).
25. C.J. Reid, J.A. Ballantine, S.R. Andrews, and F.M. Harris, Chem. Phys. **190**, 113 (1995).
26. R. L. Kelly, J. Phys. Chem. Ref. Data *16* (1987).
27. *NIST Chemistry WebBook*, NIST Standard Reference Database Number **69**, July 2001 edited by P. J. Linstrom and W. G. Mallard (National Institute of Standards and Technology, Gaithersburg MD, 20899) (http://webbook.nist.gov).
28. G. Bieri and L. Åsbrink, J. Electron Spectrosc. Relat. Phenom. **20**, 149 (1980)
29. M. Allan, E. Heilbronner, E. Kloster-Jensen, and J.P. Maier, Chem. Phys. Lett. **41**, 228 (1976).

30. K. Kimura, S. Katsumata, Y. Achiba, T. Yamazaki, and S. Iwata, "*Handbook of HeI Photoelectron Spectra of Fundamental Organic Compounds*", Japan Scientific Society Press, Tokyo (1981).
31. G. Bieri, F. Burger, E. Heilbronner, and J.P. Maier, Helv. Chim. Acta **60**, 2213 (1977) 2213.
32. G. Herzberg and J.W.C. Johns, Astrophys. J. **158**, 399 (1969).
33. J.R. Wyatt and F.E. Stafford, J. Phys. Chem. **76**, 1913 (1972).
34. M.W. Chase Jr., J. Phys. Chem. Ref. Data Monograph **9**, 1 (1998).
35. R. E. Smalley, Laser Chem. **2**, 167 (1983)
36. F. M. Devienne and M. Teisseire, Astron. Astrophys. **147**, 54 (1985)
37. P.P. Radi, T.L. Bunn, P.R. Kemper, M.E. Molchan and M.T. Bowers, J. Chem. Phys. **88**, 2809 (1988).
38. Y. Kato, T. Wakabayashi, T. Momose, and T. Shida, J. Phys. Chem. A, submitted.*

* The article was finally published in the "Journal of Mass Spectrometry Society of Japan" (Volume 53, issue 4, p 203-210).

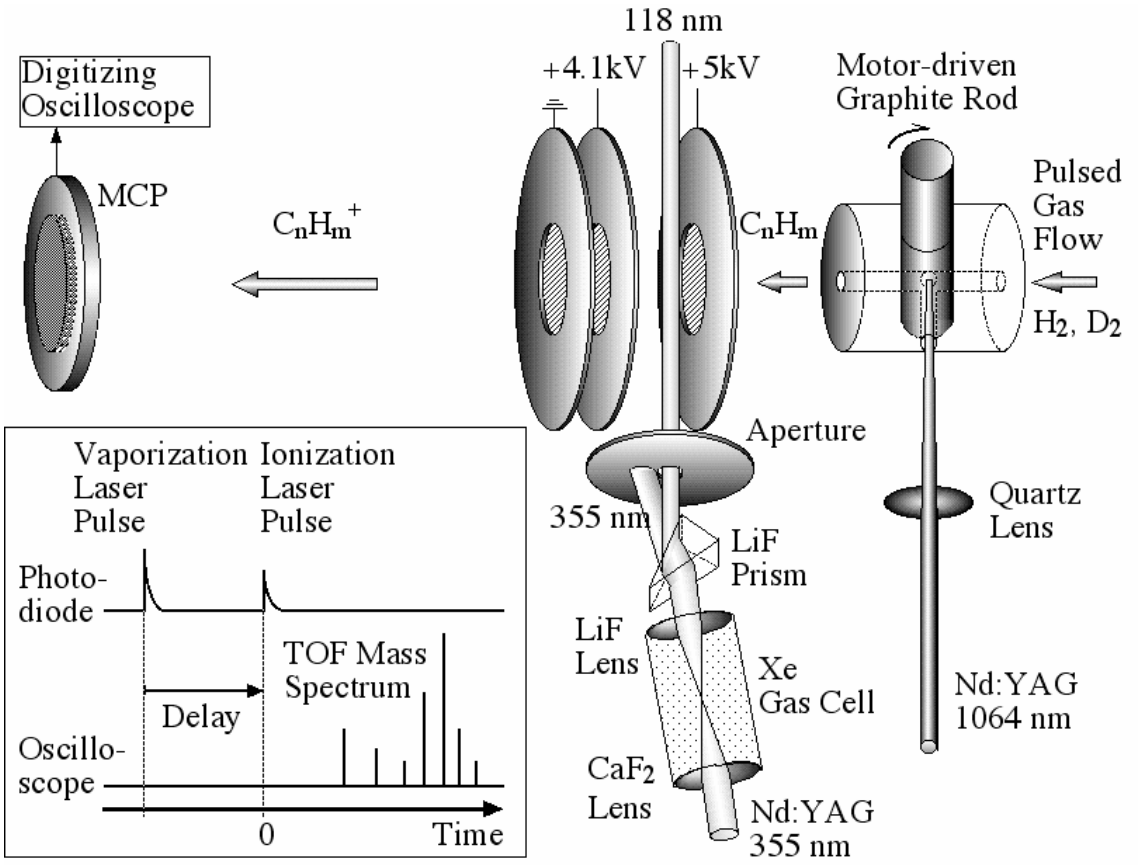

Fig. 2-1 A schematic view of the apparatus. The time sequence of the measurement is shown in the inset at the bottom left.

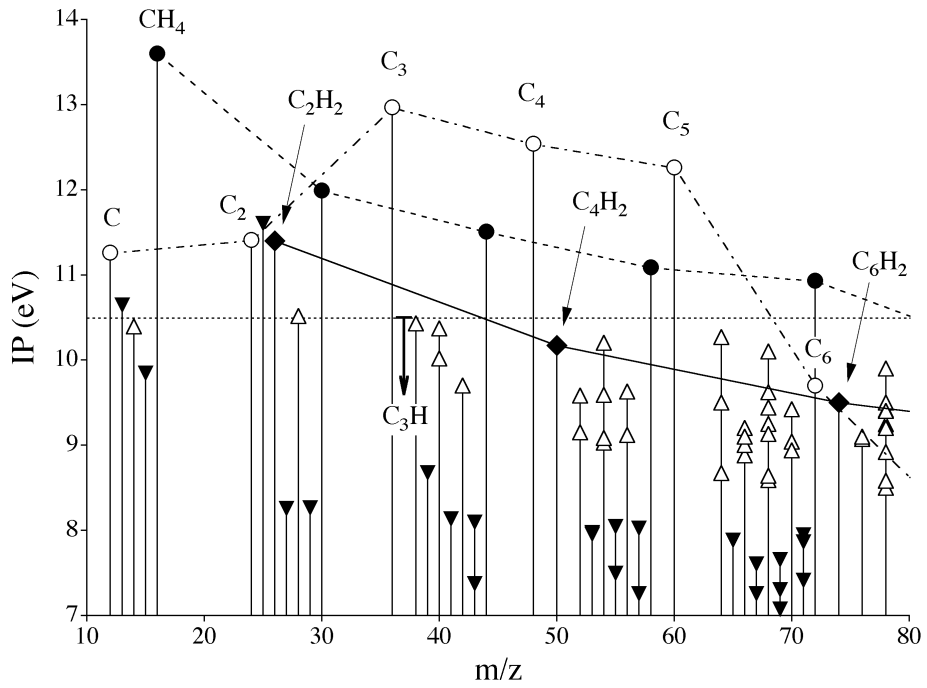

Fig. 2-2 Plot of the ionization potential (E_i) of carbon clusters C_n (open circles) and unbranched hydrocarbon molecules C_nH_{2m} (open triangles), and radicals C_nH_{2m+1} (closed triangles) as a function of their mass unit per charge number (m/z). The E_i of polyynes (diamonds) and *n*-alkanes (closed circles) are also shown. The horizontal dotted line corresponds to the energy of a 10.5 eV photon.

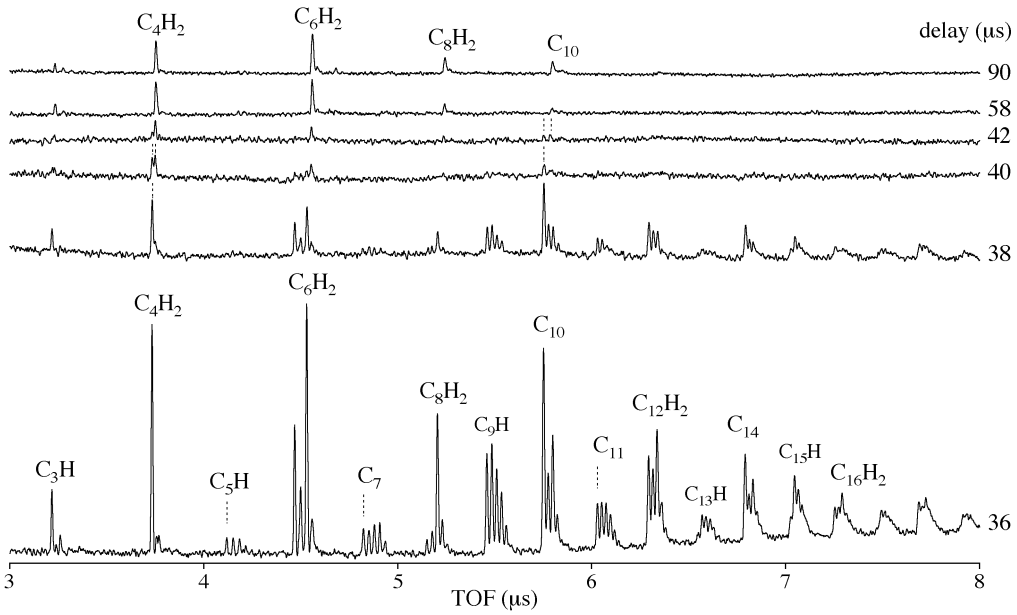

Fig. 2-3 Mass spectra of laser vaporization of graphite in H_2 gas ionized with a single-photon at 10.5 eV. The numbers to the right of the spectra represent the delay times in μs of the ionization laser pulse relative to the vaporization pulse. Vertical lines between the spectra from 38 μs through 58 μs delay indicate the shift of TOF peaks of the same molecule.

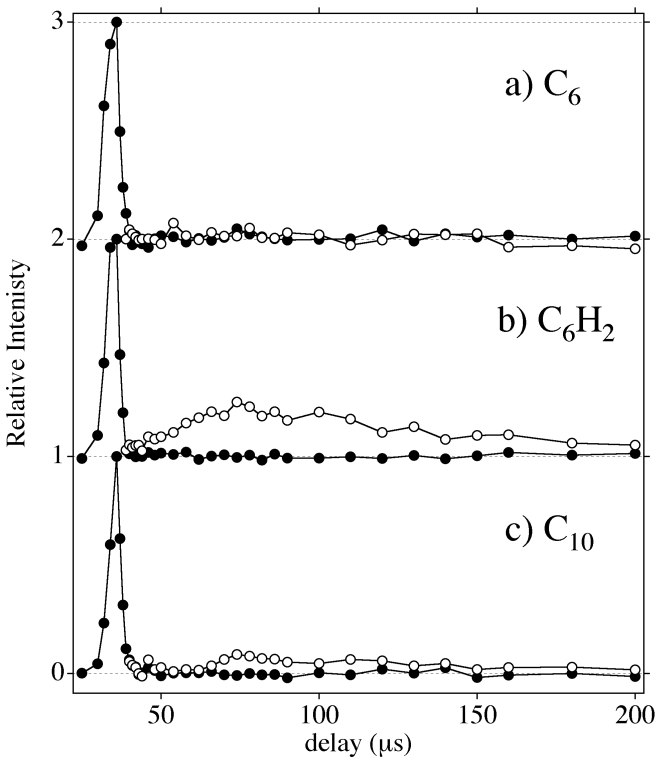

Fig. 2-4 Plot of the intensity of mass peaks of the fast (closed circles) and slow (open circles) components of (a) C_6, (b) C_6H_2, and (c) C_{10} as a function of the delay time.

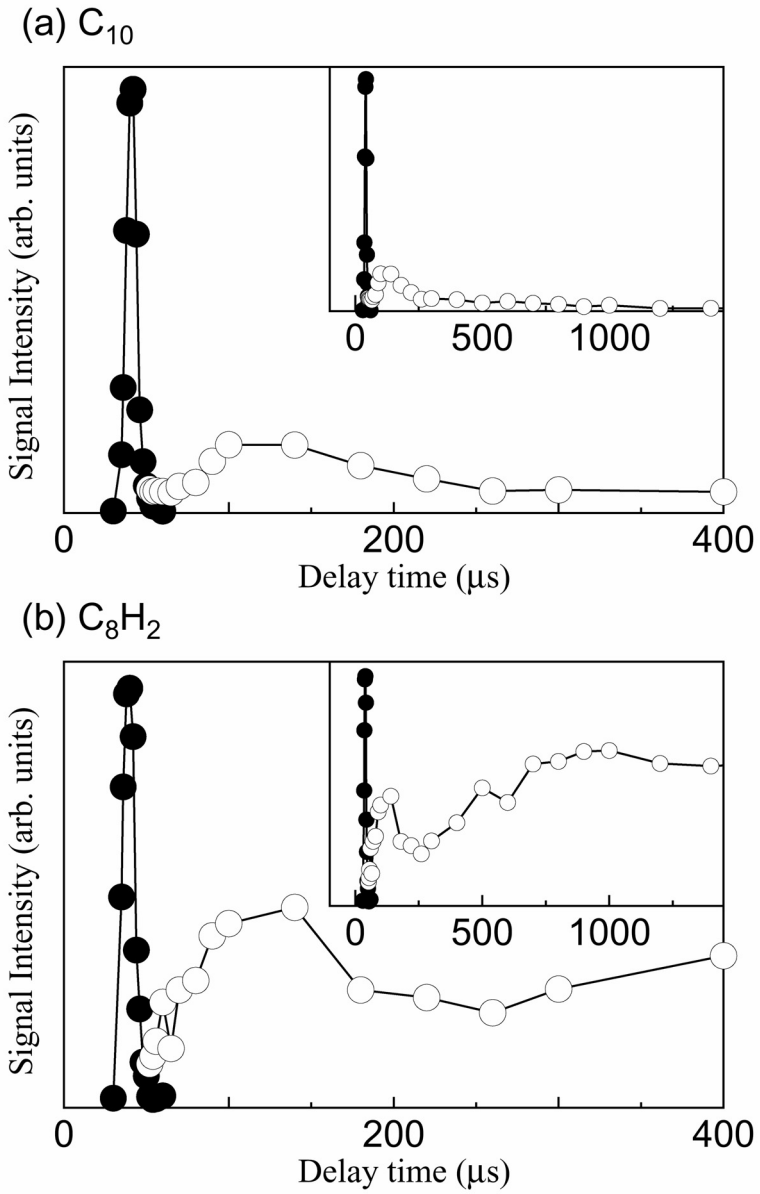

Fig. 2-5 The dissimilarity of time profiles between (a) carbon cluster (C_{10}) and (b) dihydride (C_8H_2) signal intensity for prompt component (closed circle) and delayed component (open circle) .

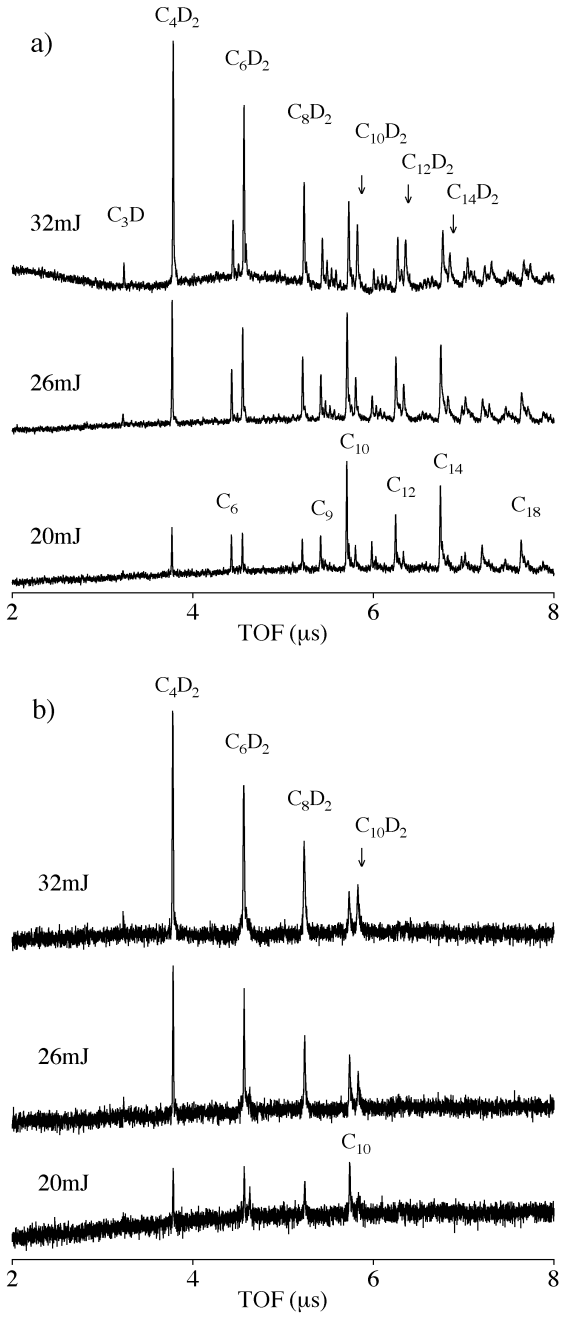

Fig. 2-6 Power dependence of the vaporization laser pulses on mass spectra in D_2 gas; (a) the fast component (46 μs delay time) and (b) the slow component (146 μs delay time). The intensity of the signals in Panel (b) is multiplied by a factor of four.

Chapter 3

Time-of-flight mass spectroscopy of carbon clusters and hydrocarbons produced by laser ablation of graphite under H_2 buffer gas: Formation and stability of C_{10} and $C_{2n}H_2$ (n=2-5)

3.1 Abstract

The products of laser ablation of graphite under the presence of H_2 gas were analyzed by time-of-flight mass spectroscopy combined with the 10.5 eV single-photon ionization technique. By changing the delay time of the pulse of an ionization laser relative to the pulse of a vaporization laser, three distinctly different velocity distributions of neutral species were identified as a result of the ablation process. The first component that appeared earlier in the ionization region consisted of various carbon clusters, C_n, and hydrocarbons, C_nH_m (n=4–20, m=1–4), while the second and third components that arrived later consisted of C_{10} and $C_{2n}H_2$ (n=2–5) only. The abundant existence of C_{10} and $C_{2n}H_2$ in the second and third components is attributable

to the stability of these molecules against collisions, which means that the detected C_{10} must be a monocyclic carbon cluster while the $C_{2n}H_2$ (n=2–5) molecules must be polyynes. Through heating the buffer gas to 600 K, the abundance of C_{10} in the third component drastically increased. The efficient production of C_{10} in the third component at high temperatures indicates that collisions between carbon clusters enhance the production of monocyclic C_{10}.

3.2 Introduction

Carbon clusters and their hydrogenated derivatives have received attention from many researchers in the fields of molecular spectroscopy, combustion chemistry, materials science, and interstellar chemistry for many years [1,2]. Among many experimental techniques, the laser ablation of graphite under the existence of various buffer gasses has been employed actively in order to investigate the structure and reactivity of carbon clusters and their derivatives [3–9]. It was found that polyynes, $HC_{2n}H$, were produced abundantly under H_2 buffer gas, while cyanopolyynes, $HC_{2n}CN$, were produced under CH_3CN and NH_3 gases [4]. The production of polyynes and cyanopolyynes by the laser ablation of graphite under these buffer gases have received attention in connection with the rich abundance of these molecules in interstellar space [10–14].

The process of laser ablation itself has been a subject in the study of non-linear gas dynamics. The dynamics of ablation products have been investigated through the use of emission spectroscopy [15,16] and fast ICCD photography [16]. The ions directly produced by the ablation process have also been studied using mass spectrometry [17–20].

These detection techniques, however, are insensitive to the ground state neutral species, which are supposed to be the most abundant products of ablation but do not emit any photon. In order to investigate these non-emissive neutral species, the photo-ionization of products followed by time-of-flight (TOF) mass spectroscopy have been employed [21].

Neutral carbon clusters produced by the laser ablation of graphite has been extensively studied employing TOF mass spectroscopy since the early work by Rohlfing et al [3]. Most of these studies employed the technique of multi-photon ionization (MPI) to ionize carbon clusters [4–6,22]. The MPI technique is a powerful one, but its drawback is that it induces serious fragmentations upon ionization. As a consequence of this fragmentation, the mass signals observed were often contaminated by the strong peaks of the fragments, so that the mass pattern observed with the MPI technique does not correspond directly to the abundance of neutral species before the ionization. In order to avoid such fragmentation, single-photon ionization via moderately weak vacuum ultraviolet (VUV) light was employed by several groups [7–9,23–26]. Single-photon ionization at 157 nm (= 7.89 eV) radiation of an F_2 laser was used for the study of fullerenes produced by laser ablation [7–9,23]. Since the radiation at 157 nm is enough to ionize fullerenes but not enough to ionize small carbon clusters, fullerenes can be selectively detected in mass spectra by ionizing with the radiation at 157 nm. In order to ionize small carbon clusters whose ionization potential is larger than 8 eV, single-photon ionization at 118 nm (= 10.5 eV), at the ninth harmonics of fundamental radiation of a Nd:YAG laser, was employed [24–27]. It was reported that mass patterns obtained by the single-photon ionization were sometimes drastically different from

those obtained by MPI in some cases [24–27]. The varying mass patterns could be attributed to the serious fragmentation by strong MPI pulses and/or the accidental resonance enhancement of the MPI process. In either event, we must be careful that the intensity of the TOF mass signal obtained by MPI may not contain information on the abundance of neutral species before ionization. Single-photon ionization should be employed for the discussion of the abundance of neutral species before ionization.

In a previous chapter [27], we reported on the study of carbon clusters, hydrocarbon molecules, and radicals produced by the laser ablation of graphite in a hydrogen (H_2 or D_2) gas expansion source studied using 10.5 eV one-photon ionization followed by time-of-flight mass spectroscopy. We observed a significant shift of TOF peaks by changing the delay time of the pulse of an ionization laser relative to the pulse of a vaporization laser. The shift of TOF peaks was interpreted as a result of the formation of two separate groups of ablation products having different initial velocities during the course of the ablation and the succeeding expansion processes. In the faster component, C_n (n=6–20) and C_nH_m (n=3–20 and m=1–4) were abundantly observed, while $C_{2n}H_2$ (n=2–5) and C_{10} existed selectively in the slower component. The separation of the ablation products was explained by the formation of a dense layer of clusters produced by laser ablation. In the present study, the TOF signal of carbon clusters and hydrocarbon molecules produced by laser ablation of graphite under the existence of H_2 buffer gas was studied more carefully in order to analyze the velocity distribution of ablation products as well as to understand the chemistry under laser ablation.

3.3 Experiments

The upper part of Figure 3-1 depicts the experimental setup of the present experiment. A graphite rod (1 cm in diameter, ^{12}C : ^{13}C = 98.9% : 1.1%) was vaporized using the second harmonics of a Q-switched Nd:YAG laser (Spectra-Physics DCR-11, 1064 nm, 7 ns duration, 7.1 mJ/pulse) in a vacuum chamber. The graphite rod was rotated slowly by a motor so that the laser ablation always occurred on a fresh surface of the rod. The pulses of the vaporization laser was loosely focused onto the graphite rod with a quartz lens whose focal length was 25 cm. The size of the spot of the vaporization laser was about 1 mm in diameter on the target surface. Products of the laser ablation were introduced into the ionization region through a short channel employing a pulsed buffer gas flow of H_2 generated by a solenoid valve (Parker-Hannifin General Valve 9-279-900). The size of the channel was 2 mm in diameter and 12 mm in length. The pressure of the H_2 gas before the valve was set at 15 atm, where the intensity of the mass signal became its maximum. The pressure of the vacuum chamber was about $1x10^{-7}$ torr without the buffer gas flow, while the pressure increased up to $1x10^{-6}$ torr with the buffer gas flow.

Products of the laser ablation were ionized by 10.5 eV (= 118 nm) pulsed radiation at 60 mm downstream of the ablation point. The 10.5 eV radiation was generated as the third harmonics of 355 nm radiation in a Xe gas cell [28,29]. The cell was made of stainless-steel whose diameter and length were 2 cm and 20 cm, respectively. The third harmonics of a Q-switched Nd:YAG laser (Continuum Powerlite 8010, 5 ns pulse width, 150 mJ/pulse) was tightly focused in the cell filled with 16 Torr of Xe gas by a CaF_2 lens (f = 10 cm at 355 nm) to generate 10.5 eV photons. The VUV radiation at

10.5 eV thus generated was paralleled by a LiF_2 lens (f = 10 cm at 118 nm), and then separated from the 355 nm radiation by an LiF prism before leading into the ionization region through an 8 mm-diameter aperture. The power of the VUV radiation was weak enough so that only single-photon ionization could occur at the ionization region.

Positive ions produced by the VUV radiation at 10.5 eV were accelerated with static electric fields created by three plates whose voltage were kept at +4.80 kV, +3.98 kV, and 0 V, respectively, as shown in Figure 3-1. The distances between the first and second electrodes, and the second and third electrodes were 2 cm and 1.5 cm, respectively. The accelerated ions were detected by multi-channel plates (Galileo 6205) placed at 75.3 cm downstream of the ionization region. The signals detected at the multi-channel plates were recorded with a digitizing oscilloscope (Tektronix TDS544A) and plotted as a function of time to obtain TOF mass spectra. All the measurements were done at the repetition rate of 10 Hz.

The time sequence of the vaporization pulse, the ionization pulse, and the recording of TOF signal by the detector is shown in the lower part of Figure 3-1. Spectra were recorded at many different time intervals between the vaporization and ionization pulses. Since ablated molecules with different initial velocities enter the ionization region at different times, the spatial distribution of molecules generated by the ablation can be obtained by changing the delay time of the ionization pulse relative to the vaporization pulse. The timings of all the instruments were controlled by delay generators (Stanford Research Systems DG535).

3.4 Results

3.4.1 Molecules detected by TOF spectroscopy

Figure 3-2 compares the TOF mass spectra of the products produced by the laser ablation of graphite under the existence of H_2 buffer gas observed at different delay times of the ionization pulse relative to the vaporization pulse. The numbers shown at the right side of each spectrum represent the delay times in units of μs. The assignment of each mass peak is given in the spectrum at the delay time of 35 μs.

Mass peaks corresponding to C_nH_m (n≥4, m=0–4) are clearly seen in the spectrum taken at the delay time of 35 μs except for those corresponding to the pure carbon clusters of C_4, C_5, and a hydrocarbon of C_4H. Since the ionization potentials of C_4 and C_5 are larger than 10.5 eV, these molecules are not able to be ionized by the single-photon at 10.5 eV [30]. In other words, the absence of the mass peaks corresponding to C_4 and C_5 clearly indicates that only single-photon ionization took place, but MPI did not take place under our experimental conditions. Therefore, the relative intensities of the TOF mass signal shown in Figure 3-2 carries information on the abundance of each neutral molecule produced by the laser ablation.

A smooth distribution of intensities of mass signals was observed for C_{2n+1}, $C_{2n+1}H$, $C_{2n+1}H_2$, $C_{2n+1}H_3$, and $C_{2n+1}H_4$ with n= 2–7. On the other hand, the intensities of C_{2n} and $C_{2n}H_2$ were observed stronger than those of $C_{2n}H$, $C_{2n}H_3$, and $C_{2n}H_4$ for n=2–6. The fact that the maximum number of hydrogen atoms m in any detected hydrocarbons of both $C_{2n}H_m$ and $C_{2n+1}H_m$ was m=4 indicates that highly unsaturated hydrocarbon molecules were formed by the ablation. The clear alternation in the intensities for even numbered clusters, $C_{2n}H_m$, indicates that dihiydrides $C_{2n}H_2$ and bared carbon clusters C_{2n} are chemically more stable than others.

At delay times longer than 65 μs, all peaks disappeared except for C_4H_2, C_6H_2, C_8H_2, $C_{10}H_2$, and C_{10}. At the delay time of 200 μs, the mass peak of C_{10} disappeared but other peaks corresponding to $C_{2n}H_2$ with n=2–5 were still able to be detected. It should be noted that the peaks of C_4H_2 and C_6H_2 still remained clearly even at the delay time of 8 ms.

3.4.2 Shift of TOF peaks

In a previous chapter, we reported on the sudden change of TOF signals of the same species by changing the delay time of the ionization pulse relative to the vaporization pulse [27]. The shift was interpreted as a result of the formation of two separate groups of ablation products having different initial velocities caused by the ablation process. In the present chapter, the shift of TOF signals was more carefully examined than the previous one. It turned out that there were actually three different velocity components, and the velocity in each component changed slightly as a function of the delay time of the ionization pulse relative to the vaporization pulse. The details are described below.

Figure 3-3 shows the expansion of the TOF mass spectra of C_4H_2, C_6H_2, and C_8H_2 at the delay times between 35 and 200 μs. The numbers shown on the right side of the spectra represent the delay time in μs. The spectral intensities were plotted with the same scale except for the spectrum observed at the delay time of 35 μs, which is multiplied by a factor of 0.025. In the spectra of C_4H_2 shown in the left panel of Figure 3-3, an intense TOF peak designated as C_4H_2 (I) was observed at the delay time of 35 μs, but its intensity decreased at 55 μs and almost disappeared at 65 μs. On the

other hand, a new peak designated as C_4H_2 (II) appeared at about 0.05 μs later TOF at the delay time of 55 μs and this remained until 100 μs. Another peak designated as C_4H_2 (III) started to appear at 70 μs and remained even at the delay time of 200 μs. All of these three peaks can be assigned to the signal of C_4H_2. The same behavior of TOF signals was also observed for both C_6H_2 and C_8H_2 as shown in the center and right panels of Figure 3-3. The shift of TOF is attributable to the difference in the initial velocity of these molecules caused by the ablation process as discussed in Sec. 5.

The upper panel of Figure 3-4 shows the change of peak intensity of C_4H_2 as a function of the delay time of the ionization pulse relative to the vaporization pulse. The closed circles (●), open circles (○), and asterisks (*) show, respectively, the intensities of the peak of C_4H_2 (I), C_4H_2 (II), and C_4H_2 (III). The intensities of C_4H_2 (II) and C_4H_2 (III) are multiplied by a factor of 20. The component C_4H_2 (I) reaches a maximum at the delay time of about 30 μs, while the components C_4H_2 (II) and C_4H_2 (III) find their maximum at about 60 μs and 90 μs, respectively.

More detailed analysis revealed that the TOF of each component changed slightly by altering the delay time as shown in the lower panel of Figure 3-4. The component C_4H_2 (I) designated as closed circles showed the change of the TOF from 6.305 μs to 6.315 μs as the delay time increased. On the other hand, the TOF of the component C_4H_2 (II) designated as open circles decreased from 6.355 μs to 6.340 μs as the delay time increased. The TOF of the component C_4H_2 (III) designated as asterisks started at 6.335 μs and approached to 6.340 μs as the delay time increased. Essentially the same shift of TOF was observed for both C_6H_2 and C_8H_2.

Panel (a) of Figure 3-5 shows the expansion of the TOF mass spectra of C_{10} and

$C_{10}H_2$ in H_2 buffer gas at various delay times. The intensity of the TOF peak of C_{10} and the shift of TOF are shown in Figure 3-6. The three components C_{10}(I), C_{10}(II), and C_{10}(III) showed the same behavior as C_4H_2; each component has one maximum in intensity, and the TOF of the first component (C_{10}(I)) increased, the TOF of the second component (C_{10}(II)) decreased, and the TOF of the third component (C_{10}(III)) approached a constant value. Panel (b) of Figure 3-5 shows the expansion of the TOF mass spectra of C_{10} in He buffer gas at various delay times for the sake of comparison. The same shift and change of TOF was observed in both H_2 and He buffer gasses. The same TOF behaviors observed for different buffer gas indicate that the shift and change of TOF shown in Figures 5 and 6 originate in the process of laser ablation itself. The origin of the shift of TOF is discussed in Sec. 5.

3.4.3 Dependence on ablation intensity

Figure 3-7 compares the mass spectra obtained with different powers of the vaporization laser. The upper three traces are the TOF mass spectra obtained with relatively weak pulses of the vaporization laser (4.0 mJ/pulse), while the lower traces are those with relatively intense pulses (7.1 mJ/pulse). Traces (a) are the spectra taken at 35 μs delay time of the ionization pulse relative to the vaporization pulse, while traces (b) and (c) are those at 65 μs and 200 μs delay times, respectively. As was previously reported [27], the intensity of C_{10} kept roughly constant irrespective of the power of the vaporization laser as seen in trace (b), for example, while the intensities of other hydrocarbons increased drastically as the powers of the vaporization laser increased. At vaporization pulses of 7.1 mJ, smaller hydrocarbons such as C_4H_2 or

C_6H_2 intensified compared with weaker vaporization pulses at 4.0 mJ. The pronounced signal of C_4H_2 and C_6H_2 indicates that these small hydrocarbons were fragmented from larger clusters.

3.4.4 Dependence on the temperature of buffer gas

The dependence of TOF signals on the temperature of buffer gas was examined using He gas. For this experiment, the cluster source made of stainless steel block was replaced with a copper tube. Details of the modified cluster source are shown in Figure 3-8. In order to change the temperature of the buffer gas, the copper tube was heated to about 1100 K with an iron-chrome wire heater. At this temperature, the actual gas temperature was about 600 K, which was measured by a thermocouple placed at the end of the copper tube. All conditions except for the modified cluster source were the same as those described in Sec. 3.

The TOF spectra observed through the heating of the buffer gas to 550 K were essentially the same as those observed at the room temperatures. On the other hand, the clear enhancement of the third component of C_{10} and C_{12} was recognized with the temperature of the buffer gas at about 600 K, as shown in Figure 3-9 (compare this with Figure 3-5 (b)). The intensity of the TOF of C_{10} observed at the temperature of 600 K is plotted in Figure 3-10 as a function of the delay time. By comparing these with the upper panel of Figure 3-6, it is clearly seen that the third component of C_{10} was drastically enhanced by heating up the buffer gas. On the other hand, only a slight enhancement of the second component relative to the first component was observed even at the temperature of 600 K.

3.4.5 Comparison between one-photon and multi-photon ionization

Figure 3-11 compares the TOF mass spectra of laser ablation products observed by one-photon ionization and those by multi-photon ionization (MPI). These experiments were conducted in He buffer gas in order to simplify the spectra. For MPI experiments, we used the third harmonics of a Nd:YAG laser (3.5eV) for ionization. The third harmonics of an unfocused pulse of 150 mJ/pulse was used to ionize the ablation products. The diameter of the ionization pulse was about 10 mm.

Trace (a) in Figure 3-11 shows the TOF spectrum obtained by 10.5 eV one-photon ionization at the delay time of 45 μs. The TOF spectrum obtained by MPI at the same delay time is shown in trace (b). Small carbon clusters such as C_2, C_3, C_4 and C_5 were clearly observed by MPI. In addition, carbon clusters larger than C_{40} were also observed. The bimodal distribution of the TOF spectrum obtained by MPI has been reported previously [3]. The most intense peak in the larger carbon clusters is C_{60} [3,9,23]. On the other hand, the bimodal distribution was not observed using 10.5 eV one-photon ionization as seen in Trace (a). Figure 3-12 shows the expansion of the TOF signal in the mass region up to C_{100} obtained through 10.5 eV one-photon ionization. Carbon clusters up to C_{80} were detected, but the signal intensities of larger carbon clusters were 100 times smaller than the signal of C_{10}. The bimodal distribution of ion signals in the TOF spectrum by MPI shown in trace (b) of Figure 3-11 may be attributed to the fragmentation of C_{40}–C_{120} from much larger clusters caused by intense MPI pulses. In any case, clusters larger than C_{40} did not exist abundantly in our cluster source as the neutral species produced by the laser ablation before the ionization.

Traces (c) and (d) of Figure 3-11 show the TOF produced by MPI at the delay times of 100 μs and 160 μs, respectively. Carbon clusters larger than C_{40} disappeared at the delay time of 100 μs, but appeared again at the delay time of 160 μs. The TOF signals of carbon clusters larger than C_{40} remained until 250 μs of the delay time, but disappeared again after 250 μs. On the other hand, carbon clusters smaller than C_{30} were always observed until the delay time of 4 ms.

Figure 3-13 shows the peak intensities and the shift of the TOF of C_{60} observed by MPI. The fullerene C_{60} observed after 160 μs of the delay time seen in Figure 3-11 can be attributed to the third component (III) but not to the second component (II), as the shift of TOF in this component increased as a function of the increase in the delay time (see Figures 3-4 and 3-6). Both of the components (I) and (III) had a single maximum in intensity. The maximum intensity of C_{60} in the component (III) was observed at the delay time of 160 μs.

3.5 Analysis and Discussion

3.5.1 Shift of TOF

One of the important findings of the present research was the shift in TOF by changing the delay time of the ionization pulse relative to the vaporization pulse as shown in Figures 3-4, 3-6, and 3-13. The shift of TOF should be attributed to the difference in initial velocities of ablated species. As shown in Figure 3-1, the direction of the beam of buffer gas through the cluster source was collinear with the axis of ion acceleration in the present experiment. Therefore, products of ablation could possess certain velocity distributions towards the axis of the acceleration. The distribution of

initial translational velocities along the axis before the acceleration must be the origin of the peak shift of TOF mass spectra.

For the Wiley-McLaren type of time-of-flight mass spectrometer [31] employed in the present work, the flight time t of a molecule with mass m and charge q can be expressed analytically as follows [31].

$$t = \frac{\sqrt{2m}}{qE_1}\left(\sqrt{U_0 + qx_1E_1} \pm \sqrt{U_0}\right) + \frac{\sqrt{2m}}{qE_2}\left(\sqrt{U_0 + qx_1E_1 + qx_2E_2} - \sqrt{U_0 + qx_1E_1}\right) + x_3\sqrt{\frac{m}{2\left(U_0 + qx_1E_1 + qx_2E_2\right)}} + t_0 \qquad (1)$$

In Eq. (1), U_0 is the initial translational energy of a molecule defined as $U_0 = \frac{1}{2}mv_0^2$, where v_0 is the initial velocity of the molecule. The symbols x_1, x_2 and x_3 represent the distances, and E_1 and E_2 are the electric fields as shown in Figure 3-1. The last term t_0 in Eq. (1) is the offset of time, which is mainly caused by the delay of electrical circuits. The plus sign in the first term of the right-hand-side of Eq. (1) is for the case when the initial velocity v_0 is negative, while the minus sign is for positive.

When m and v_0 are small enough so that U_0 is smaller than qx_1E_1, the following approximation can be applied.

$$\sqrt{U_0 + qx_1E_1} \cong \sqrt{qx_1E_1} \qquad (2)$$

$$\sqrt{U_0 + qx_1E_1 + qx_2E_2} \cong \sqrt{qx_1E_1 + qx_2E_2} \qquad (3)$$

These assumptions are valid for our experimental setup, since $qx_1E_1 = 8.5\times10^{-17}$ $\mathrm{kgm^2s^{-2}}$ (x_1= 13 mm, and $E_1 = 4.1\times10^4$ $\mathrm{Vm^{-1}}$) while, for example, $U_0 = 4.0\times10^{-19}$ $\mathrm{kgm^2s^{-2}}$ for v_0= 2000 $\mathrm{ms^{-1}}$ of C_{10}. With these approximations, the flight time t can be simplified as follows.

$$t \cong \left\{ \sqrt{\frac{2x_1}{qE_1}} + \frac{\sqrt{2}}{qE_2}\left(\sqrt{qx_1E_1 + qx_2E_2} - \sqrt{qx_2E_2}\right) + \frac{x_3}{\sqrt{2\left(qx_1E_1 + qx_2E_2\right)}} \right\} m^{1/2} - \frac{1}{qE_1} v_0 m + t_0$$

$$\equiv \alpha m^{1/2} - \beta v_0 m + t_0 \qquad (4)$$

In the second line of Eq. (4), the symbols α and β are the coefficients of the first and second term of the right-hand side of the first line of Eq. (4). The values α and β and the offset t_0 are determined only by the instrumental settings, but do not depend on molecules. Consequently, the flight time can be described by the sum of two terms, one is proportional to $m^{1/2}$ and the other is proportional to mv_0.

The coefficients in Eq. (4) calculated from the values of the present instrumental setup were $\alpha = 2.1\times10^7$ $\mathrm{kg^{-1/2}s}$ and $\beta = 1.5\times10^{14}$ $\mathrm{kg^{-1}m^{-1}s^2}$, and $t_0 = 2.5\times10^{-8}$ s. It was confirmed that our observed TOF spectra can be analyzed completely within experimental errors for molecules with any mass by Eq. (4) adopting the values of the coefficients given in the above. From the analysis of the observed TOF by the use of Eq. (4), the initial velocities of molecules at any delay time were calculated. The initial velocities thus determined are also given on the right side of the lower panels of Figures 3-4, 3-6 and 3-13.

3.5.2 Split of ablated plumes

As described in Sec 4, three bunches of ablated species were observed. The motion of each bunch can be surmised by the initial velocities obtained by the use of Eq. (4). As seen in Figures 3-4, 3-6 and 3-13, the first bunch (component (I)) had initial velocities of 3000 – 500 ms^{-1} towards the detector. The third bunch (component (III)) had initial velocities of 500 – 0 ms^{-1} towards the detector. On the other hand, the second bunch (component (II)) had initial velocities of 1000 – 0 ms^{-1}. The negative velocity means that the second bunch was moving backwards.

The splitting of plumes produced by laser ablation has been studied for various conditions both experimentally and theoretically [16,32–36]. It has been demonstrated that there are two types of bunch-separation in the propagation of ablated plumes. One is the separation due to the formation of a Knudsen layer [32–36], and the other is the separation due to the generation of a shockwave [16,32,33].

The formation of a Knudsen layer is induced by collisions among the ablated species at the initial stage of gas expansion [34,35]. In front of the Knudsen layer, ablation products expand adiabatically, so that the ablation products moves rapidly from the ablation surface to the vacuum. On the other hand, it is known that there exists another component near the target surface that does not escape from the ablation surface quickly. This component is often referred to as a Knudsen layer. The formation of the Knudsen layer is characteristic of the laser ablation process, which forms even under the vacuum without the buffer gas [32,33,37]. Ablation products in the Knudsen layer are compressed by the flow of the buffer gas. Thus we conjecture that the compression of the Knudsen layer by buffer gas results in the formation of a dense layer of carbon

clusters, which moves rather slowly. As a result, the formation of the dense layer of carbon separates the ablation plume in two; one is the component in front of the layer which expands adiabatically, and the other is the component behind the layer which moves slowly due to the existence of the layer.

The second type of separation is due to the generation of a shockwave in the adiabatically expanding region [33]. It occurs only under the existence of the buffer gas. Collisions between rapidly propagating species and buffer gas cause the turbulence resulting in the formation of the shockwave. Once the shockwave is generated, it is known that the adiabatically expanding region is separated into two components, one is the forward-moving component and the other is the stopped/backward-moving component [16,32,33].

The bunch-separations observed in our study must result from the same phenomena as those observed in the general ablation process described above. Thus, we conjecture that the first and second components ((I) and (II)) were in front of the dense layer of carbon, while the third component (III) was behind the layer. In front of the dense layer, the generation of the shockwave further separated the components into two, one is the forward-moving component (component (I)) and the other is the stopped/backward-moving component (component (II)). This diagram explains the observed shift and change of TOF shown in Figures 3-4, 3-6, and 3-13.

The first component (I) expanded almost freely without heavy collisions. Thus, the TOF mass spectra of the component (I) must carry the information on the chemical species produced by the initial ablation process. On the other hand, molecules in the second component (II) are subjected to heavy collisions with other molecules and buffer

gas due to the resulting turbulence. Also, there must be many collisions in the third component (III) due to the existence of the dense layer in front of the component. Thus, molecules observed in the second and third components were produced as a result of fragmentation, clustering and chemical reactions which were induced by collisions during the expansion. Molecules detected in the second and third components, then, must be stable against collisions.

3.5.3 Molecules in component (I)

Molecules in the first component (I) were almost free from collisions. Thus the TOF mass spectra obtained through one-photon ionization must carry the information on the abundance of molecules produced by the vaporization pulses.

Bared carbon clusters C_n for n=6–15 were clearly observed at the delay time of 35 μs as shown in Figure 3-2. In addition, larger clusters up to C_{100} were continuously observed in the first component (I), as shown in Figure 3-12. These carbon clusters were produced at a very early stage of the ablation and the succeeding expansion processes. Therefore, most of these molecules must be ejected directly from the graphite surface as a result of an vaporization pulse.

Under H_2 buffer gas, hydrocarbons of C_nH_m for m=1–4 were also observed. The abundance of these hydrocarbons in the first component (I) increased by increasing the power of vaporization pulses as shown in Figure 3-7. The temperature of ablation plumes of graphite is known to be 2500 – 4000 K [15]. At such high temperatures, hydrogen molecules would thermally decompose into hydrogen atoms [38]. An increase in the abundance of hydrocarbons at higher power of vaporization pulses clearly

indicates that the thermally decomposed hydrogen atoms, but not hydrogen molecules, mainly reacted with carbon clusters to form these hydrocarbons. The formation of hydrocarbons C_nH_m for m=1–4 by laser ablation of graphite under hydrogen gases (H_2 and D_2) were discussed in the previous chapter [27].

It is natural to consider that hydrogenated derivatives observed in the first component (I) must have similar structures with their parent carbon clusters. An unbranched linear chain or monocyclic ring would be predictable as stable structures for carbon clusters C_n of n≤30 [39–42]. Carbon clusters with monocyclic ring structures are chemically stable, and they do not react with hydrogen atoms easily. Thus, the hydrocarbons observed in the first component (I) must have a structure of unbranched linear chain. Thermally decomposed hydrogen atoms may attack each end of linear C_n molecules to form C−H chemical bonds. The fact that dihydrides $C_{2n}H_2$ were abundantly observed for clusters with even numbers of carbon atoms indicates that these dihydrides were polyacetylene (H−(C=C)$_n$−H), which is chemically stable. On the contrary, linear carbon clusters with odd numbers of carbon atoms, C_{2n+1}, have a cumulenic form (:C(=C=)$_{2n-2}$C:), and thus any hydrocarbons $C_{2n+1}H_m$ up to m=4 were produced by the reaction with hydrogen atoms.

3.5.4 Molecules in components (II) and (III)

Molecules in the second (II) and third (III) components were subjected to heavy collisions with other molecules and the buffer gas. Thus molecules observed in these components must be stable against collisions.

As shown in Figure 3-2, dihydrides $C_{2n}H_2$ for n=2–5 were observed even at the

delay time of 8 ms. It is reasonable because of the inert property of polyacetylene (H−(C=C)$_n$−H). Collisions with carbon clusters do not destroy these polyacetylene molecules easily.

In addition to the polyacetylene molecules, carbon clusters of C_{10} were selectively observed in the components (II) and (III). If these were linear in structure, it would not survive against collisions with hydrogen atoms and other carbon clusters. Thus, the carbon cluster C_{10} observed in the components (II) and (III) must be monocyclic C_{10}. It is predicted that the monocyclic form is more stable than the linear chain for C_{10} [40–44]. The signal of C_{10} faded away faster than the signals of the polyacetylene molecules as shown in Figure 3-2. Thus, monocylclic C_{10} must be fairly stable against collisions, but not as stable as the polyacetylene molecules.

The existence of C_{10} in the components (II) and (III) may also be accounted for by the selective fragmentation of monocyclic C_{10} from larger carbon clusters or the dense layer of carbon. Several studies suggest that large carbon clusters at high temperature produce C_{10} preferentially as fragments during their cooling processes [45–47]. Such selective fragmentation may also explain the selective signal of C_{10} at longer delay times [27].

3.5.5 Enhancement of C_{10} at high temperatures

As shown in Figures 3-9 and 3-10, the abundance of C_{10} in the component (III) increased drastically by heating the buffer gas up to 600 K. On the contrary, no enhancement of C_{10} was observed in the components (I) and (II). Thus, warm buffer gas accelerates the formation of carbon cluster C_{10} only behind the dense layer of

carbon. More collisions between the buffer gas and ablated species are expected at higher temperatures. These collisions may induce selective fragmentation of monocyclic C_{10} from larger carbon clusters or the dense layer of carbon more efficiently. Also, the dense layer of carbon itself must be heated due to the compression by the heated buffer gas. As a result, the warm dense layer of carbon may fragment monocyclic C_{10} more efficiently, which resulted in the increase of the signal of C_{10} in the third component.

It has been reported that the high temperature (about 1300 K) of the reaction region is indispensable for the efficient production of fullerenes, in general [48–50]. As shown in Figure 3-13, C_{60} was also observed in the third component. Since Figure 3-13 displays the results of MPI, the existence of signal of C_{60} in the third component does not mean that C_{60} existed as the neutral products before the ionization. However, it must be true that precursor molecules of C_{60} existed abundantly in the third component. Although we do not observe a clear enhancement of the signal of C_{60} or other fullerenes at the temperature of 600 K with one-photon ionization, the enhancement of C_{10} behind the dense layer of carbon at higher temperatures may have a connection with fullerene formation. More experiments are needed for further discussion.

3.5.6 Signals of C_{60} observed by MPI

Using the MPI technique, TOF signals of larger carbon clusters C_n with n>40 were clearly observed in addition to the smaller carbon clusters shown in Figure 3-11. On the other hand, such larger carbon clusters were not observed clearly in the 10.5 eV

one-photon ionization. It is well-known that the intense TOF signal of C_{60} with MPI has led to the discovery of fullerenes [3,22]. However, the fact that the intensities of the TOF signal of larger carbon clusters obtained by one-photon ionization indicates that these larger clusters and fullerenes do not exist abundantly as the initial neutral species of the ablation products. Stronger signals of fullerenes using MPI may be a result of the fragmentation of fullerenes from much larger clusters or the dense layer of carbon with intense MPI pulses.

3.6 Conclusions

Neutral species produced by the laser ablation of graphite under H_2 buffer gas were characterized by time-of-flight mass spectroscopy combined using the 10.5 eV one-photon ionization technique. The observed TOF spectra clearly indicated that the ablated plumes split into three bunches, the first component expanded adiabatically having a large forward velocity, the second component flew backwards due to the turbulence caused by the collision with the buffer gas, and the third component moved slowly behind the dense layer of carbon. In the second and third components, ablated species were subjected to heavy collisions with other molecules as well as with the buffer gas, so that only the chemically inert molecule survived. As a result, polyacetylene ($H-(C=C)_n-H$) with n=2–5 and a bared carbon cluster C_{10} were selectively observed in the second and third components. The stability of C_{10} implies that it must be monocylcic C_{10}. By heating the buffer gas, the abundance of C_{10} in the third component increased, which suggest that the monocyclic C_{10} were also produced selectively by the fragmentation of larger carbon clusters or the dense layer of carbon.

The existence of C_{60} in the third component may indicate the relation between the monocyclic C_{10} and the formation of fullerene. The present research is the first identification of the dynamics of neutral species produced by the laser ablation of graphite.

References

1. W. Weltner, Jr. and R. J. Van Zee, Chem. Rev. **89**, 1713 (1989).
2. A. Van Orden and R. J. Saycally, Chem. Rev. **98**, 2313 (1998).
3. E. A. Rohlfing, D. M. Cox, and A. Kaldor, J. Chem. Phys. **81**, 3322 (1984).
4. J. R. Heath, Q. Zhang, S. C. O'Brien, R. F. Curl, H. W. Kroto, and R. E. Smalley, J. Am. Chem. Soc. **109**, 359 (1987).
5. H. W. Kroto, J. R. Heath, S. C. O'Brien, R. F. Curl, and R. E. Smalley, Astrophys. J. **314**, 352 (1987).
6. M. Doverstål, B. Lindgren, U. Sassenberg, and H. Yu, Z. Phys. D **19**, 447 (1991).
7. R. P. Hallet, K. G. McKay, S. P. Balm, A. W. Allaf, H. W. Kroto, and A. J. Stace, Z. Phys. D **34**, 65 (1995).
8. Q. L. Zhang, S. C. O'Brien, J. R. Heath, R. F. Curl, H. W. Kroto, and R. E. Smalley, J. Phys. Chem. **90**, 525 (1986).
9. E. A. Rohlfing, J. Chem. Phys. **93**, 7851 (1990).
10. B. E. Turner, Astrophys. J. **163**, L133 (1971).
11. L. W. Avery, N. W. Broten, J. M. MacLeod, T. Oka, and H. W. Kroto, Astrophys. J. **205**, L173 (1976).
12. H. W. Kroto, C. Kirby, D. R. M. Walton, L. W. Avery, N. W. Broten, J. M. MacLeod, and T. Oka, Astrophys. J. **219**, L133 (1978).
13. N. W. Broten, T. Oka, L. W. Avery, J. M. MacLeod, and H. W. Kroto, Astrophys. J. **233**, L105 (1978).
14. M. B. Bell, P. A. Feldman, S. Kwok, and H. E. Matthews,, Nature 295, 389 (1982).

15. E. A. Rohlfing, J. Chem. Phys. **89**, 6103 (1988).
16. A. A. Puretzky, D. B. Geohegan, R. E. Haufler, R. L. Hettich, X.-Y. Zheng, and R. N. Compton, AIP conference proceedings **288**, 365 (1993).
17. L. A. Bloomfield, M. E. Geusic, R. R. Freeman, and W. L. Broun, Chem. Phys. Lett. **121**, 33 (1985).
18. A. Kasuya and Y. Nishina, Phys. Rev. B **28**, 6571 (1983).
19. Y. A. Yang, P. Xia, A. L.. Junkin, and L. A. Bloomfield, Phys. Rev. Lett. **66**, 1205 (1991).
20. P. Pradel, P. Monchicourt, J. J. Laucagne, M. Perdrix, and G. Watel, Chem. Phys. Lett. **158**, 412 (1989).
21. T. G. Dietz, M. A. Duncan, D. E. powers, and R. E. Smalley, J. Chem. Phys. **74**, 6511 (1981).
22. H. W. Kroto, J. R. Heath, S. C. O'Brien, R. F. Curl, and R. E. Smalley, Nature **318**, 162 (1985).
23. D. M. Cox, K. C. Reichmann, and A. Kaldor, J. Chem. Phys. **88**, 1588 (1988).
24. K. Kaizu, K. Kohno, S. Suzuki, H. Shiromaru, T. Moriwaki, and Y. Achiba, J. Chem. Phys. **106**, 9954 (1997).
25. T. Wakabayashi, T. Momose, and T. Shida , J. Chem. Phys. **111**, 6260 (1999).
26. Y. Kato, T. Wakabayashi, and T. Momose, J. Chem. Phys. **118**, 5390 (2003).
27. Y. Kato, T. Wakabayashi, and T. Momose, Chem. Phys. Lett. **386**, 279 (2004).
28. A. H. Kung, J. F. Young, and S. E. Harris, Appl. Phys. Lett. **22**, 301 (1973).
29. J. F. Ward and G. H. C. New, Phys. Rev. **185**, 57 (1969).
30. R. Ramanathan, J. A. Zimmerman, and J. R. Eyler, J. Chem. Phys. **98**, 7838 (1993).

31. W. C. Wiley and I. H. McLaren, Rev. Sci. Instr. **26**, 1150 (1955).
32. D. B. Geohegan, App. Phys. Lett. **60**, 2732 (1992).
33. S. S. Harilal, C. V. Bindhu, M. S. Tillack, F. Najmabadi, and A. C. Gaeres, J. App. Phys. **93**, 2380 (2003).
34. R. Kelly, Phys. Rev. A **46**, 860 (1992).
35. R. Kelly and R. W. Dreyfus, Surf. Sci. **198**, 263 (1988).
36. R. Kelly, J. Chem. Phys. **92**, 5047 (1990).
37. Y.-K. Choi, H.-S. Im, K.-W. Jung, Int. J. Mass Spectrom. **189**, 115 (1999).
38. M. W. Chase Jr., J. Phys. Chem. Ref. Data, Monograph **9** , 1 (1998).
39. S. Yang, K. J. Taylor, M. J. CrayCraft, J. Conceicao, C. L. Pettiette, O. Cheshnovsky, and R. E. Smalley, Chem. Phys. Lett. **144**, 1988 (431).
40. K. S. Pitzer and E. Clementi, J. Am. Chem. Soc. **81**, 4477 (1959).
41. R. Hoffmann, Tetrahedron **22**, 521 (1966).
42. J. Hutter, H. P. Luethi, and F. Diedrich, J. Am. Chem. Soc. **116**, 750 (1994).
43. K. Raghavachari and J. S. Binkley, J. Chem. Phys. **87**, 2191 (1987).
44. C. Liang and H. F. Shaefer III, J. Chem. Phys. **93**, 8844 (1990).
45. T. Wakabayashi, T. Momose, T. Shida, H. Shiromaru, M. Ohara, and Y. Achiba, J. Chem. Phys. **107**, 1152 (1997).
46. P. P. Radi, T. L. Bunn, P. R. Kemper, M. E. Molchan, and M. T. Bowers, J. Chem. Phys. **88**, 2809 (1988).
47. T. Moriwaki, K. Kobayashi, M. Osaka, M. Ohara, H. Shiromaru, and Y. Achiba, J. Chem. Phys. **107**, 8927 (1997).
48. T. Guo, P. Nikolaev, A. G. Rinzler, D. Tomnek, D. T. Colbert, and R. E. Smalley, J.

Phys. Chem. **99**, 10694 (1995).

49. T. Wakabayashi, D. Kasuya, H. Shiromaru, S. Suzuki, K. Kikuchi, and Yoji Achiba, Z. Phys. D **40**, 414 (1997).

50. D. Kasuya, T. Ishigaki, T. Suganuma, Y. Ohtsuka, S, Suzuki, H. Shiromaru, Y. Achiba, and T. Wakabayashi, Eur. Phys. J. D **9**, 355 (1999).

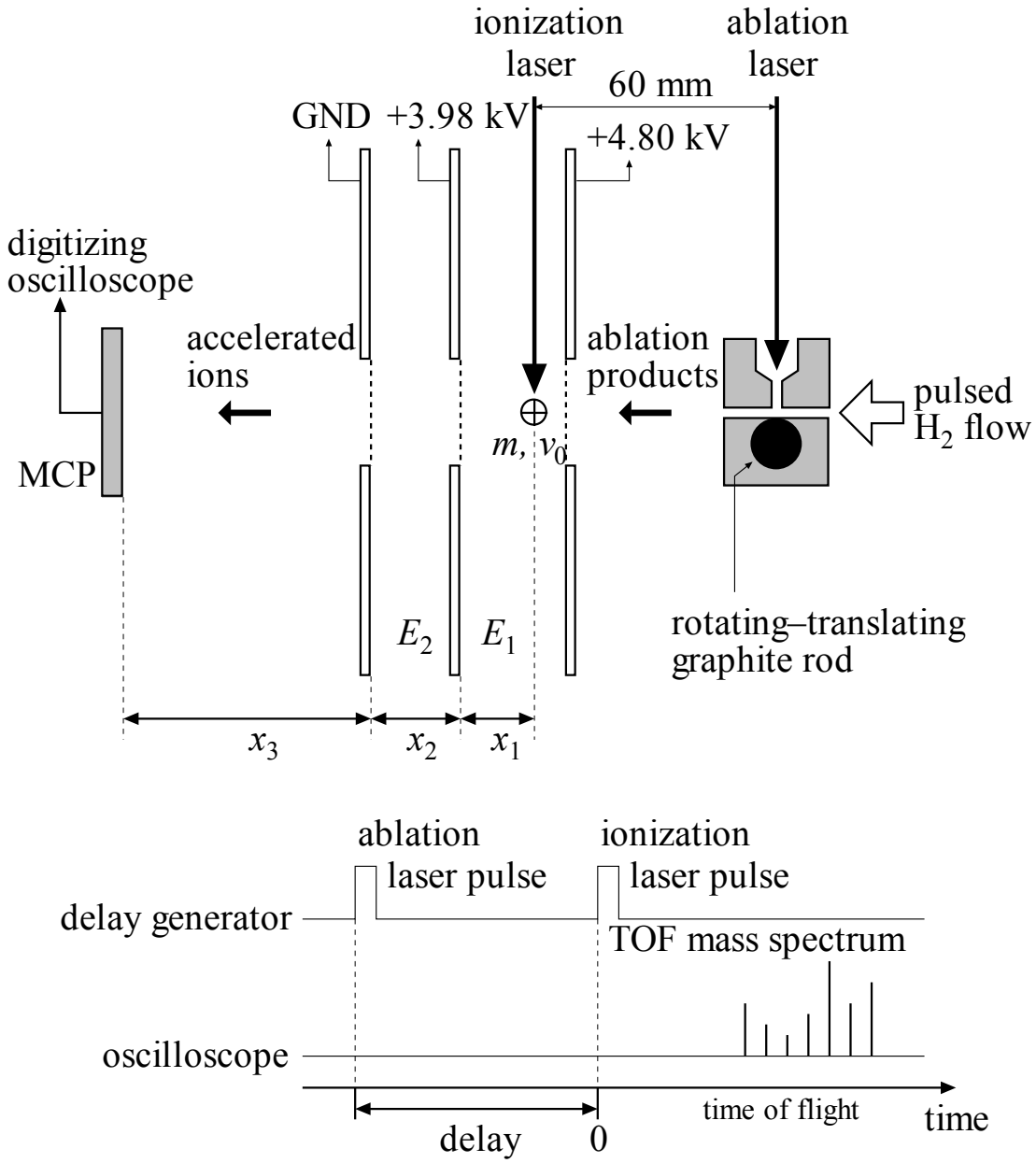

Fig. 3-1 A schematic view of the TOF apparatus. The time sequence of the measurement is shown in lower part.

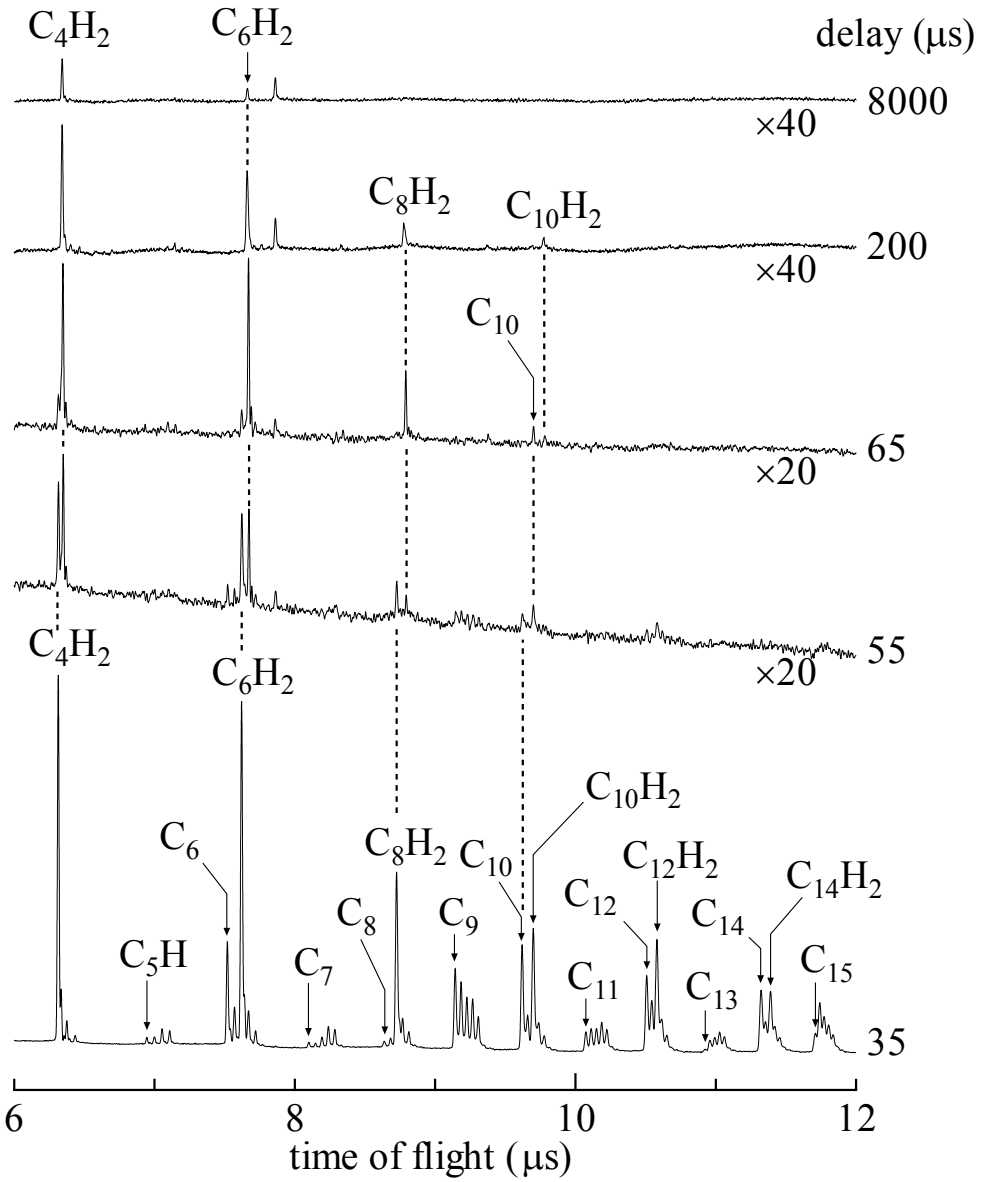

Fig. 3-2 TOF mass spectra of laser ablation of graphite in H_2 gas ionized with a single-photon at 10.5 eV. The numbers to the right of the spectra represent the delay times in μs of the ionization laser pulse relative to the ablation pulse. Spectra observed at the delay times of 55 μs and 65 μs are expanded by a factor of 20, and those at 200 μs and 8000 μs are expanded by 40. Assignments of each TOF peaks are given in the spectra observed at 35 μs. Vertical lines between the spectra indicate the shift of TOF peaks of the same molecules.

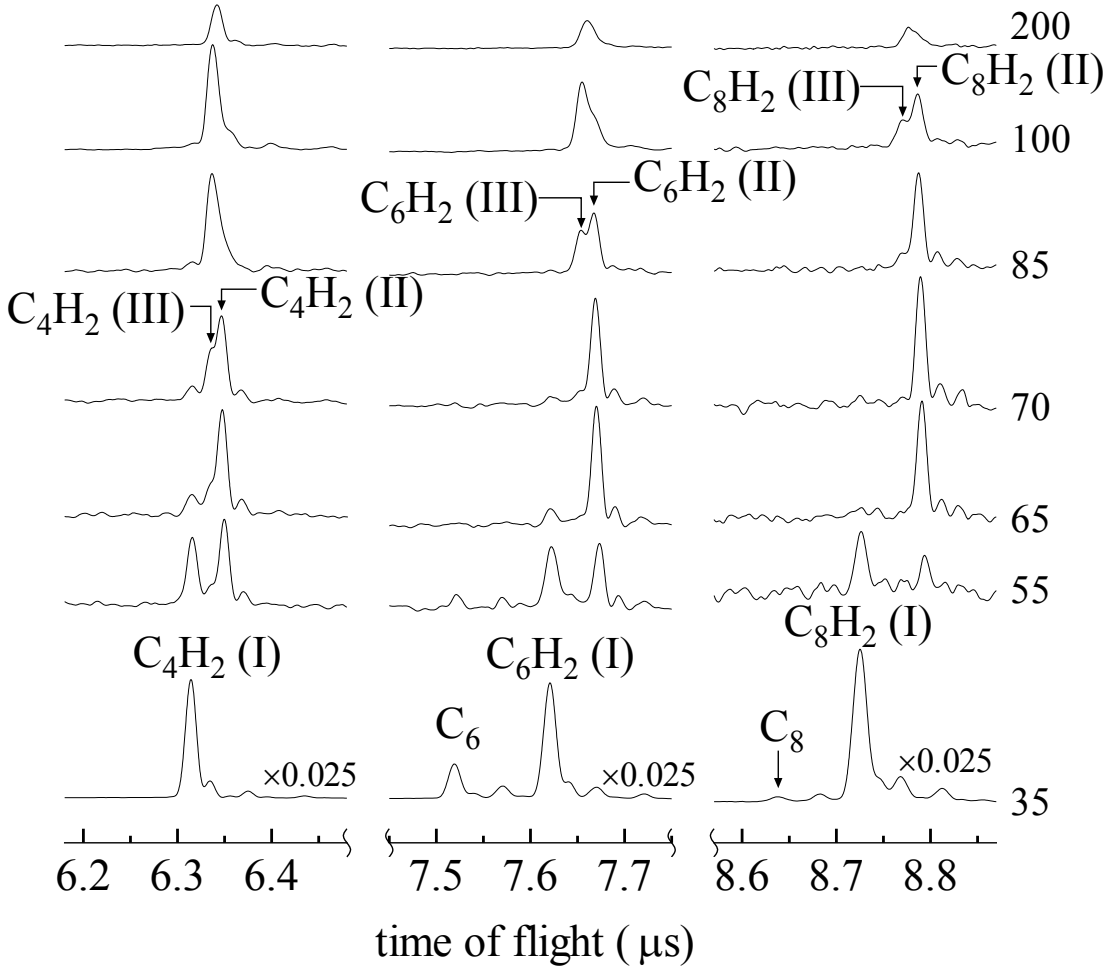

Fig. 3-3 Expansion of the TOF mass spectra shown in Figure 3-1 in the spectral regions of C_4H_2 (left), C_6 and C_6H_2 (center), and C_8 and C_8H_2 (right). The numbers to the right of the spectra represent the delay times in μs of the ionization laser pulse relative to the ablation pulse. Spectra observed at the delay time of 35 μs are multiplied by a factor of 0.025. The symbols (I), (II), and (III) after the assignments of molecules represent the first, second, and third components, respectively, of ablation plumes (see text).

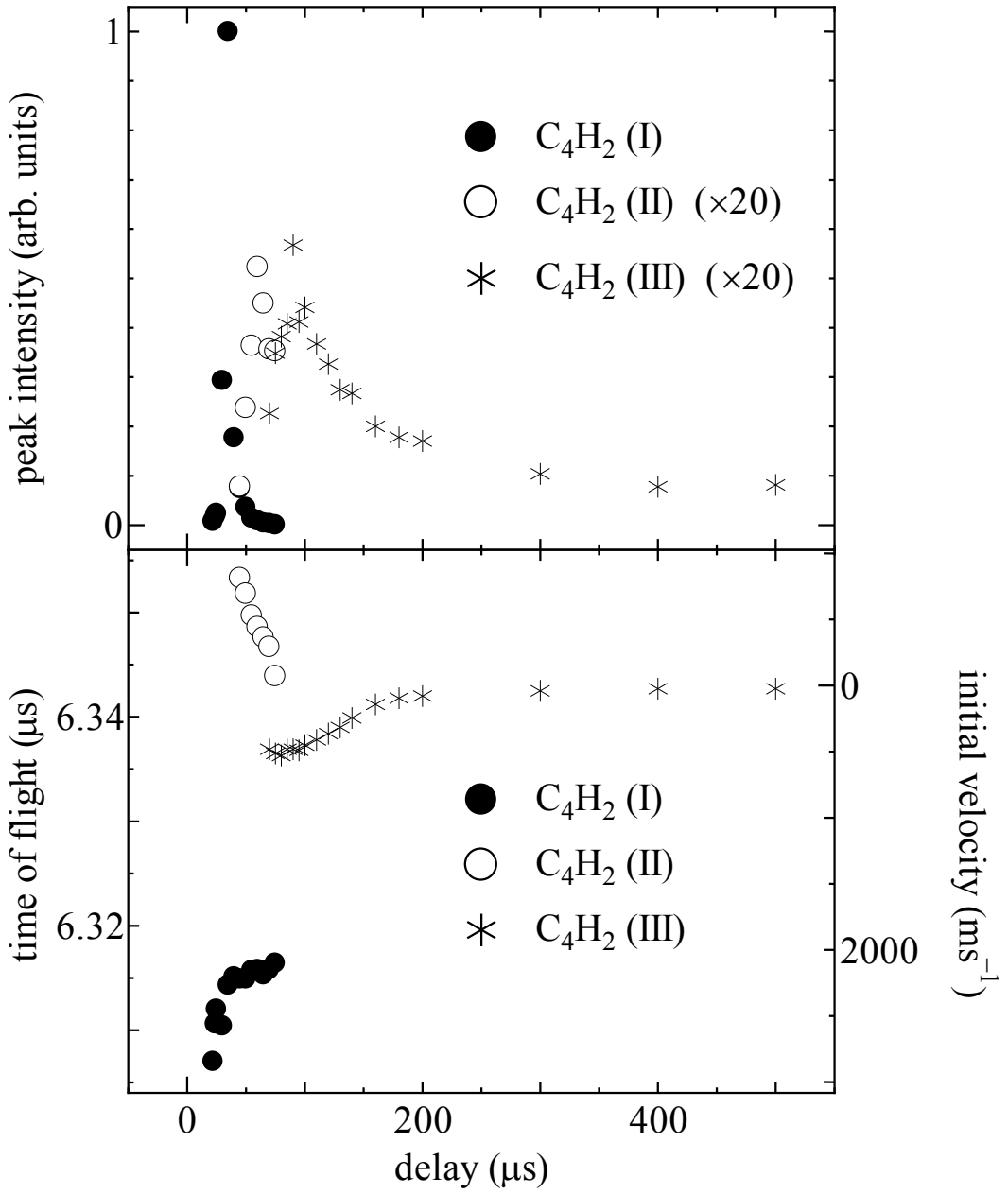

Fig. 3-4 Change of peak intensity (top) and shift of TOF (bottom) of C_4H_2 as a function of the delay time of ionization pulse relative to the ablation pulse. Signals corresponding to the first (I), second (II), and third (III) components are displayed as closed circles (●), open circles (○) and asterisks (*), respectively. The peak intensities of the second and third components are multiplied by a factor of 20.

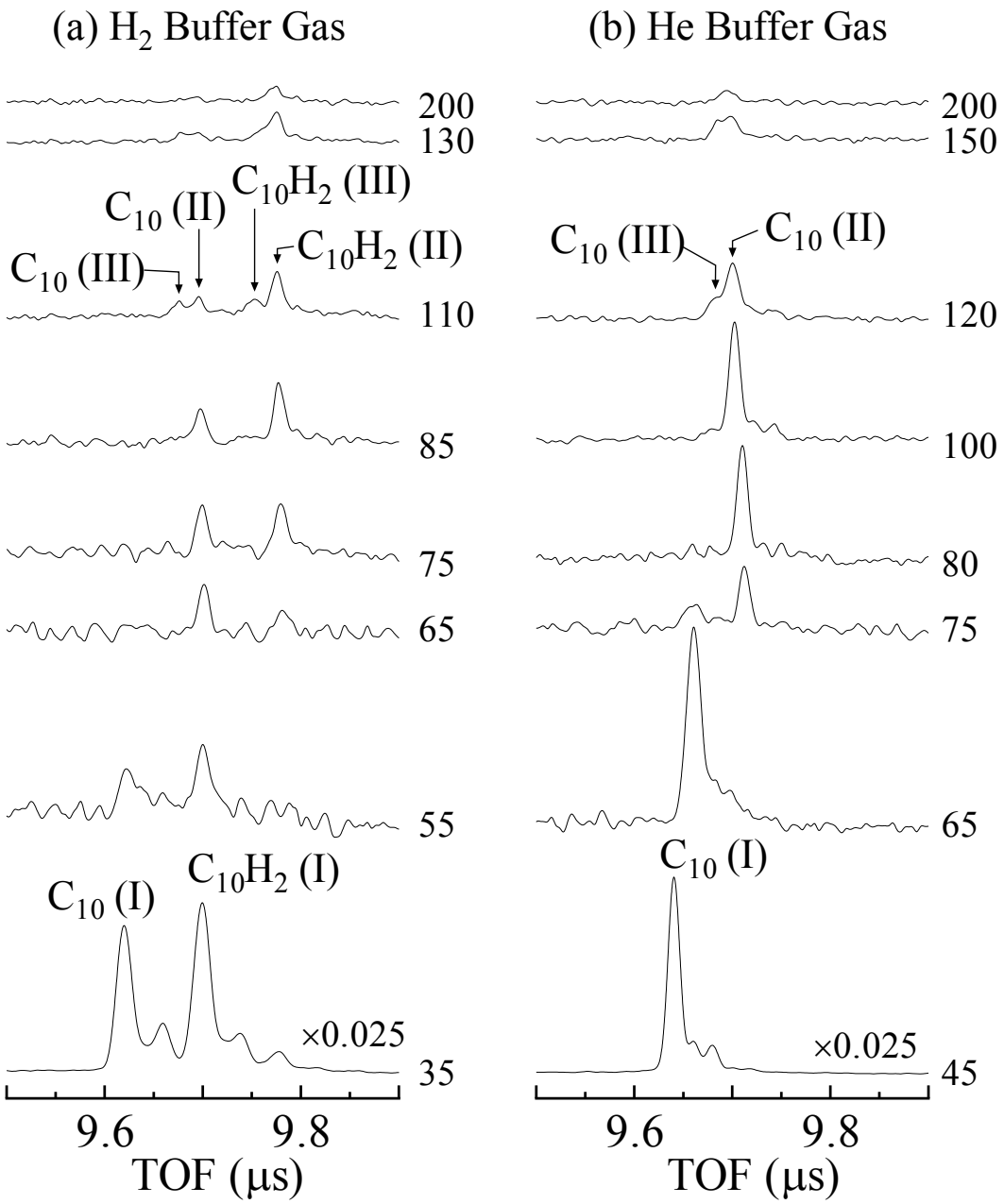

Fig. 3-5 Comparison of TOF spectra in the region of C_{10} observed in H_2 buffer gas (left) with those in He buffer gas (right). The numbers to the right of the spectra represents the delay times in μs of the ionization laser pulse relative to the ablation pulse. Spectra observed at the delay time of 35 μs are multiplied by a factor of 0.025.

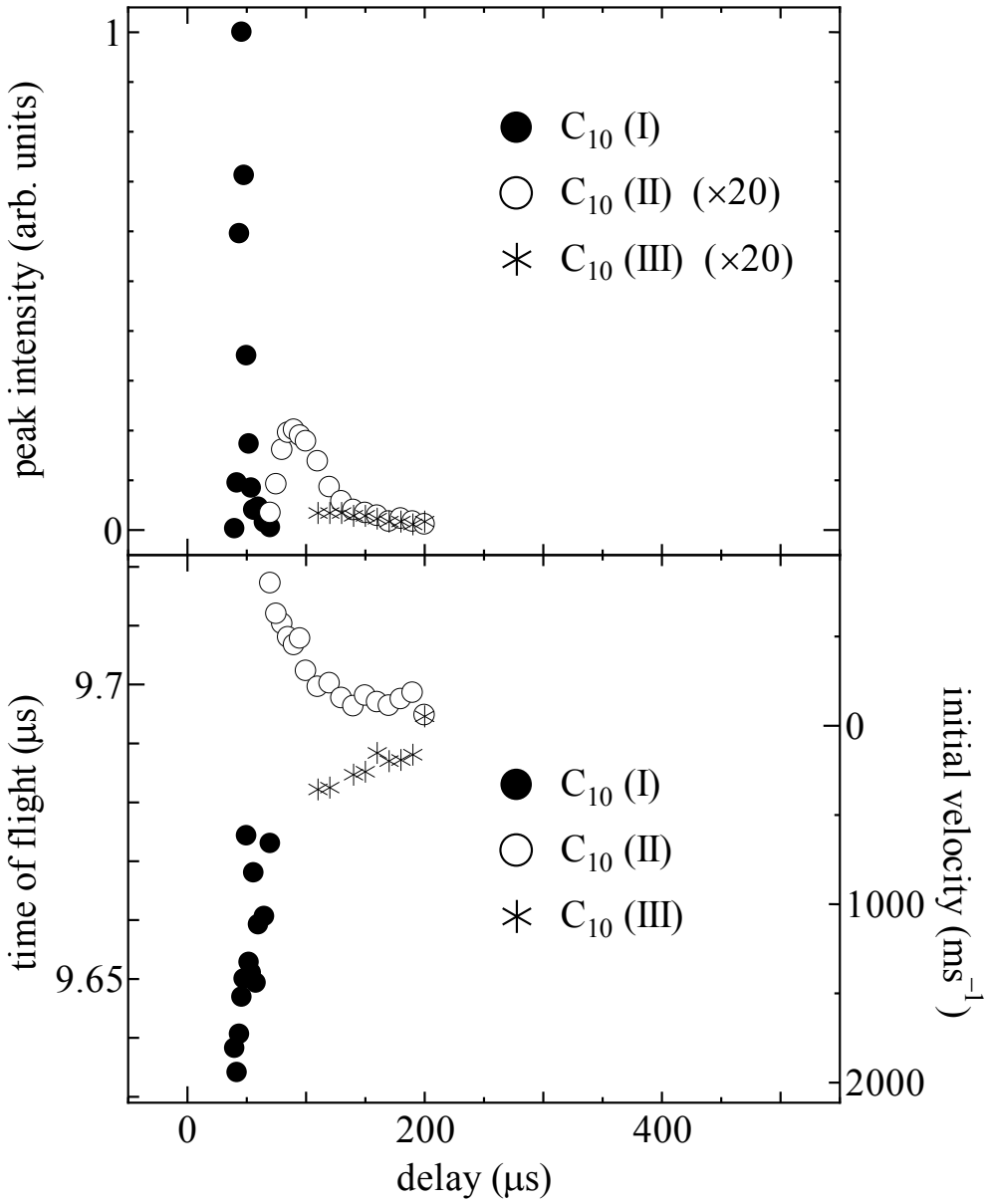

Fig. 3-6 Change of peak intensity (top) and shift of TOF (bottom) of C_{10} as a function of the delay time of ionization pulse relative to the ablation pulse observed in He buffer gas with one-photon ionization. Signals corresponding to the first (I), second (II), and third (III) components are displayed as closed circles (●), open circles (○) and asterisks (*), respectively. The peak intensities of the second and third components are multiplied by a factor of 20.

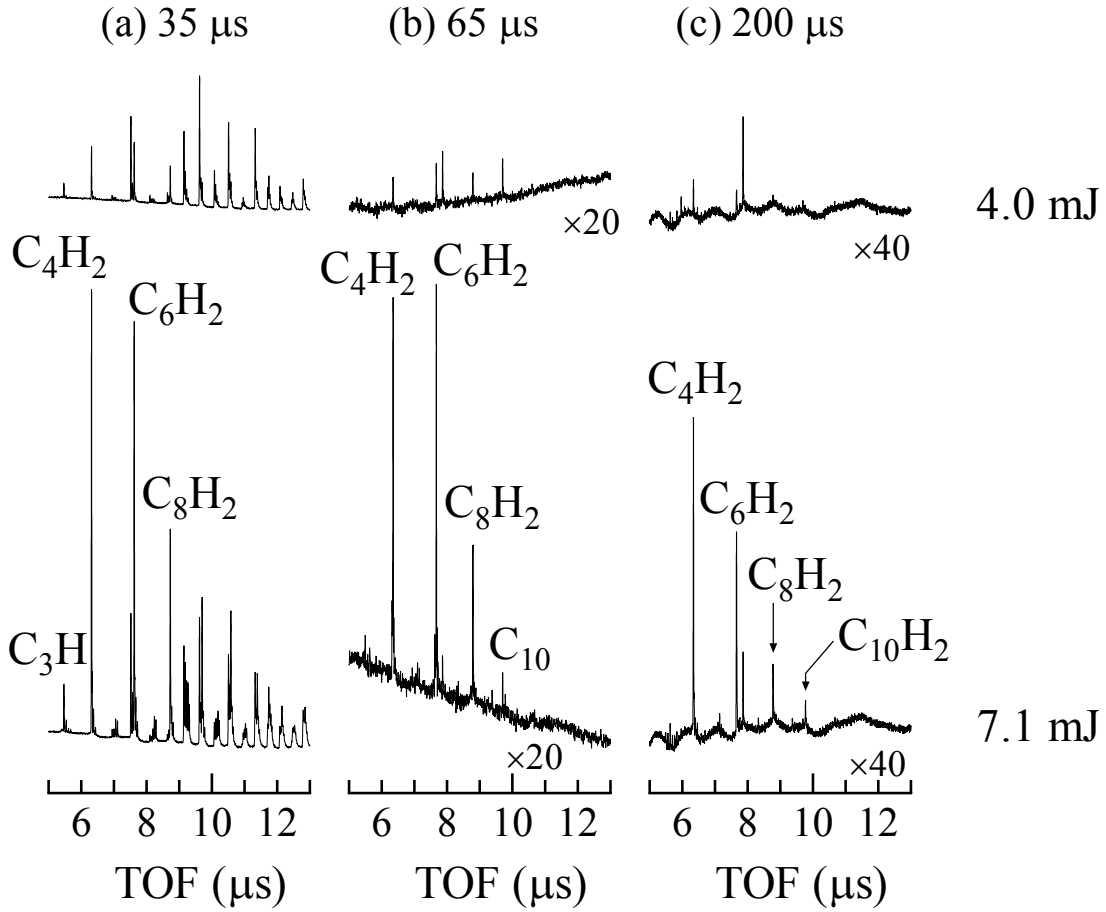

Fig. 3-7 Power dependence of the ablation laser pulses on mass spectra in H_2 buffer gas; (a) the delay time of 35 μs, (b) the delay time of 65 μs, and (c) the delay time of 200 μs. Top spectra were obtained with the ablation power of 4.0 mJ/pulse, and bottom spectra were obtained with the ablation power of 7.1 mJ/pulse.

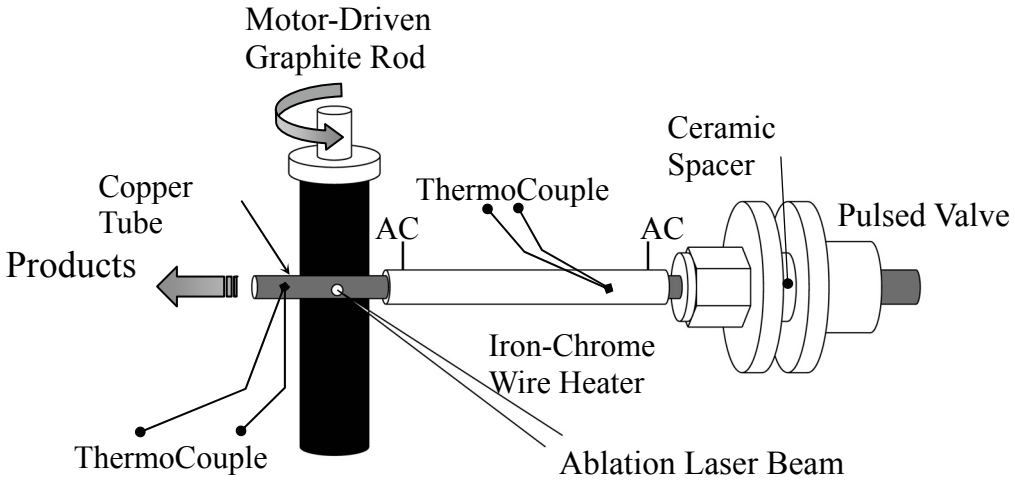

Fig. 3-8 A schematic view around the modified cluster source for the experiments of heated buffer gas. The copper tube placed after the pulsed valve was heated by a wire heater up to 1100 K. When the copper tube was heated up to 1100 K, the temperature of the buffer gas was about 600 K, which was measured by a thermocouple placed just after the exit of the gas through the cupper tube.

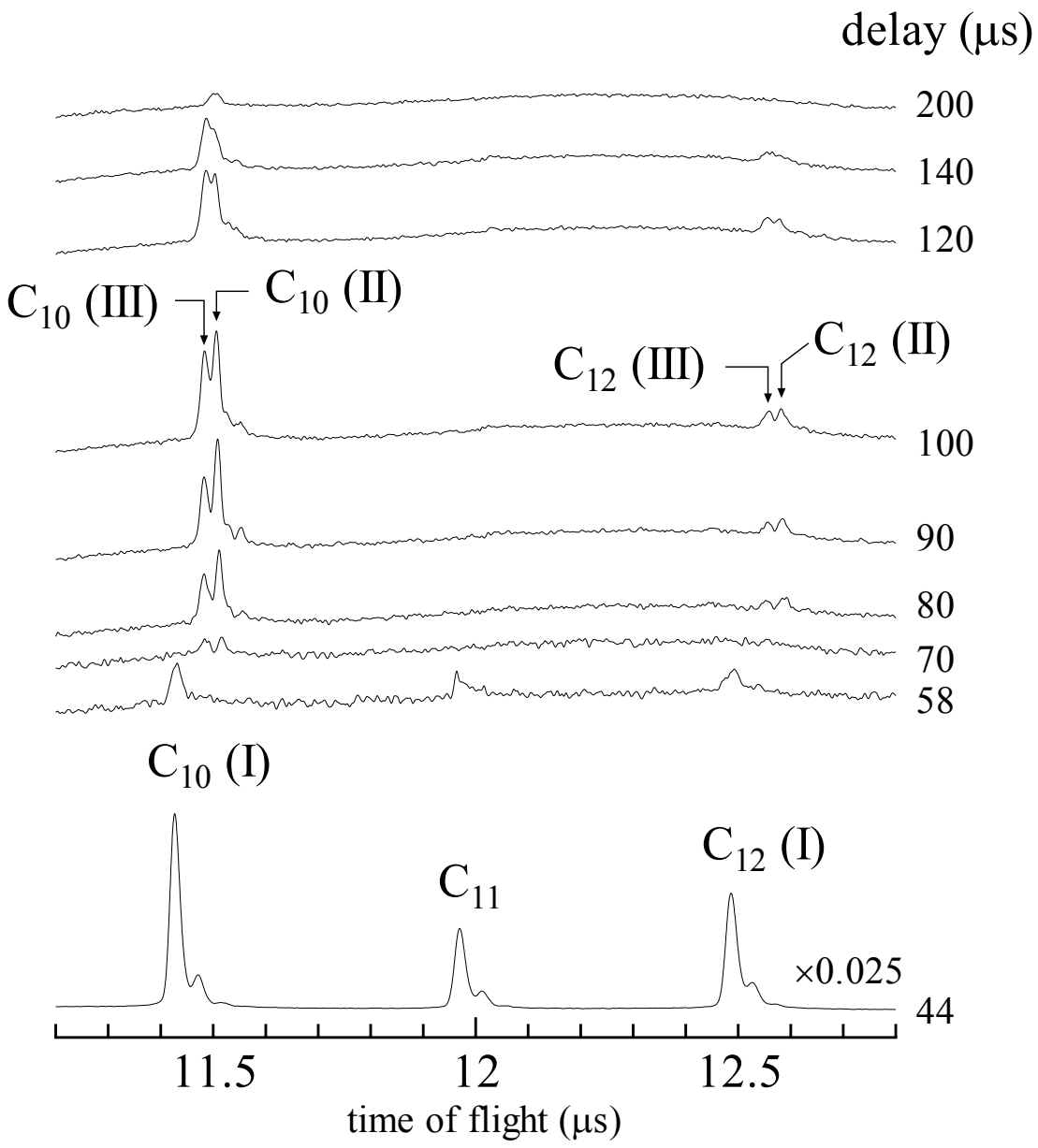

Fig. 3-9 TOF mass spectra of laser ablation of graphite in heated He gas observed by one-photon ionization. The temperature of the buffer gas at the exit was about 600 K. Only the spectral region of C_{10}, C_{11} and C_{12} is shown. The numbers to the right of the spectra represent the delay times in μs of the ionization laser pulse relative to the ablation pulse. The spectrum observed at the delay time of 35 μs is multiplied by a factor of 0.025.

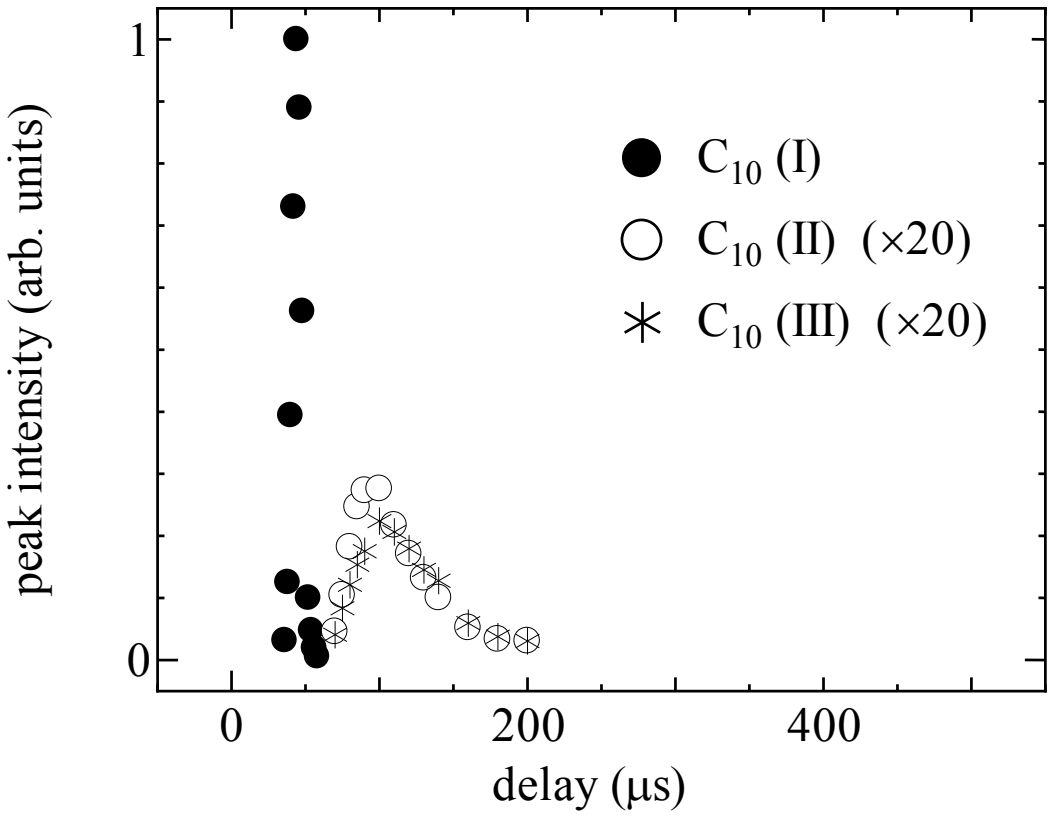

Fig. 3-10 Change of peak intensity of C_{10} observed in heated He buffer gas with one-photon ionization. The temperature of the buffer gas at the exit was about 600 K. Signals corresponding to the first (I), second (II), and third (III) components are displayed as closed circles (●), open circles (○) and asterisks (*), respectively. The peak intensities of the second and third components are multiplied by a factor of 20.

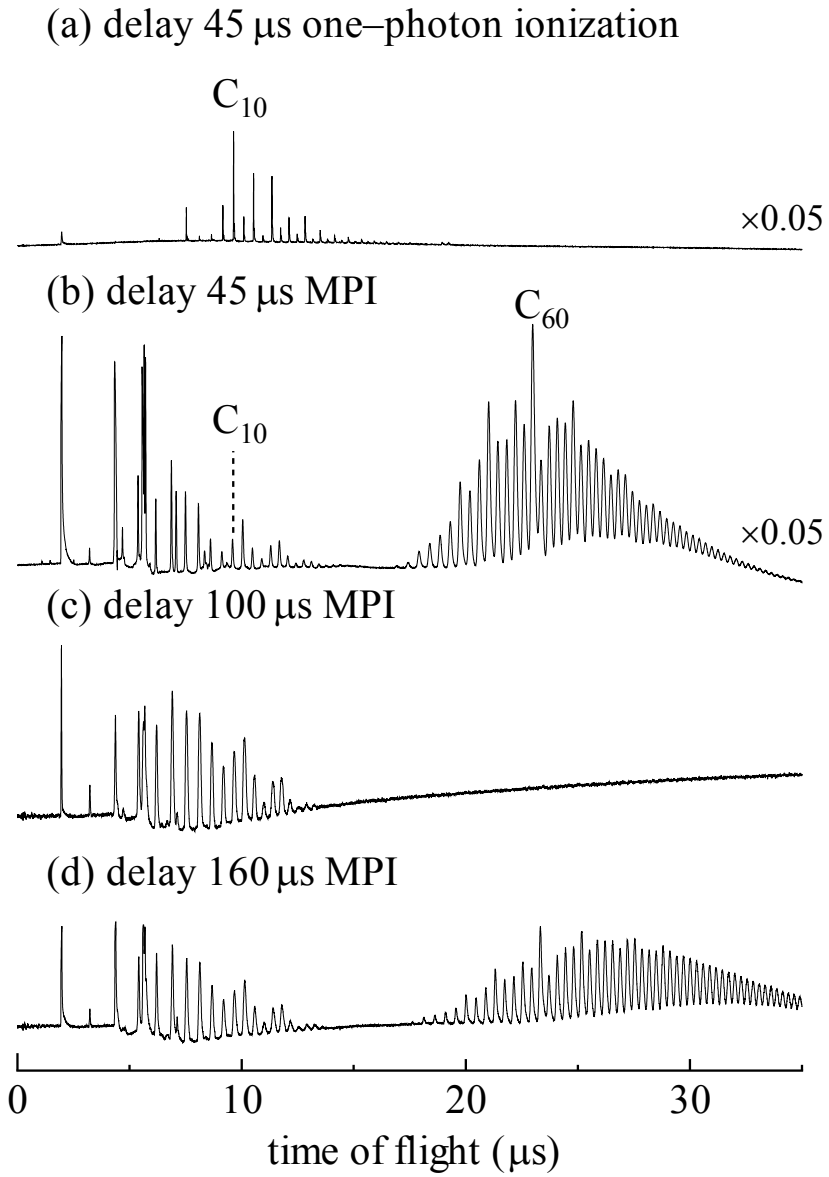

Fig. 3-11 TOF mass spectra of laser ablation of graphite in He buffer gas.

(a) Observed with the 10.5 eV one-photon ionization at the delay time of 45 μs.

(b) Observed with MPI at the delay time of 45 μs.

(c) Observed with MPI at the delay time of 100 μs.

(d) Observed with MPI at the delay time of 160 μs.

The spectra observed at the delay time of 45 μs ((a) and (b)) are multiplied by a factor of 0.05.

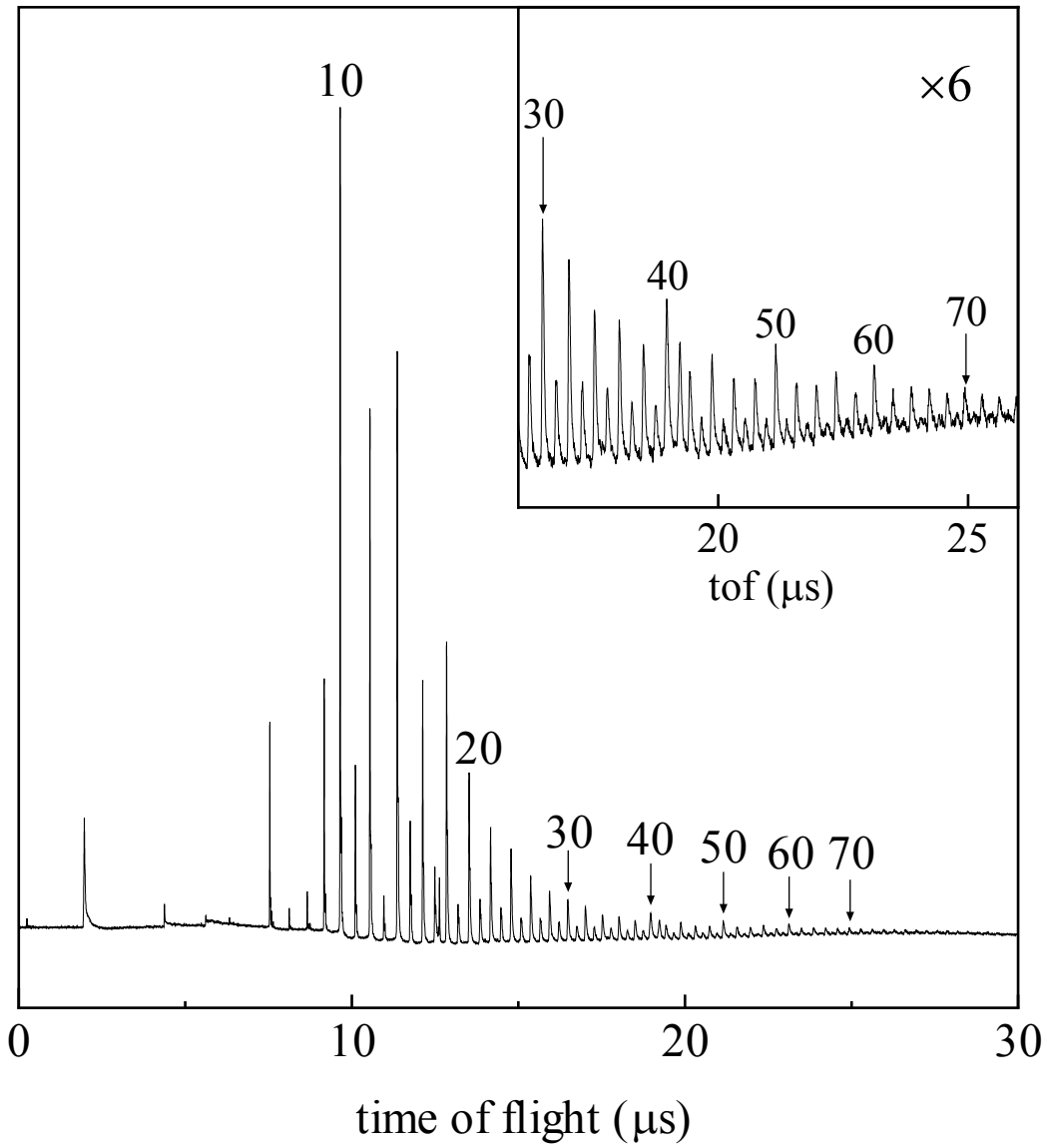

Fig. 3-12 Expansion of the TOF mass spectra observed in He buffer gas with the 10.5 eV one-photon ionization. Numbers in the trace represents the assignment of number of carbon atoms in the clusters. The inset is the expansion of the spectrum in the mass region of C_{30} and C_{70}.

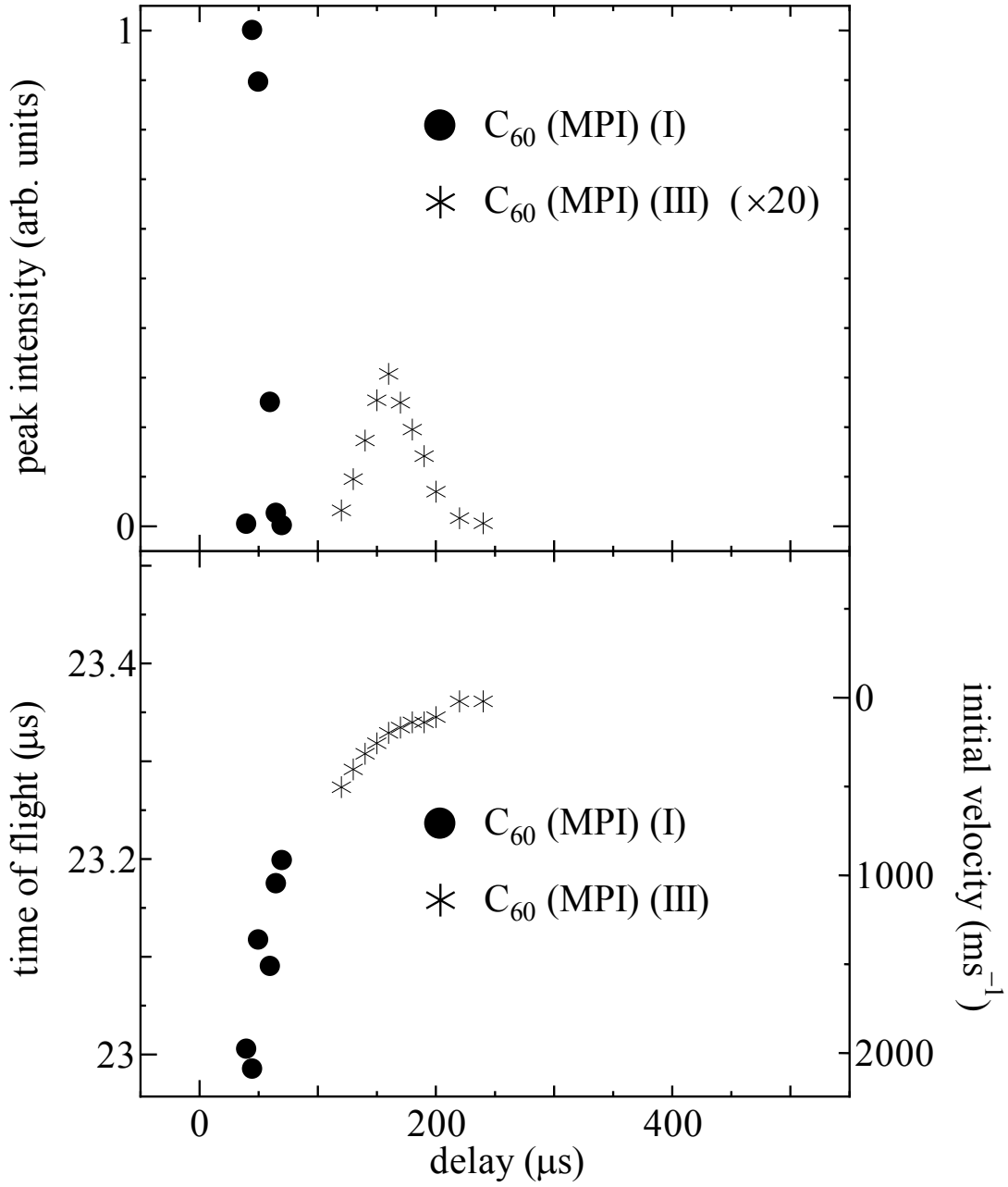

Fig. 3-13 Change of peak intensity (top) and shift of TOF (bottom) of C_{60} observed in He buffer gas with MPI. Signals corresponding to the first (I) and third (III) components are displayed as closed circles (●) and asterisks (*) respectively. The peak intensities of the third component are multiplied by a factor of 20.

Summary of the Thesis

Laser ablation of graphite in helium or hydrogen buffer gas was studied by time-of-flight mass spectroscopy for the purpose of investigating laser ablation process and the structures and reactivity of ablation products. Neutral carbon clusters C_n and their hydrogenated derivatives C_nH_m produced with Smalley type laser ablation cluster source were identified by Wiley-McLaren type time-of-flight mass spectrometer. Employed single-photon ionization technique using ninth harmonics of Nd:YAG laser (10.5 eV = 118 nm) had brought the better time-of-flight mass spectra reflecting true distribution of produced C_n and C_nH_m without the effect of multiphoton process such as photo-induced fragmentation than multiphoton ionization method.

Under He atmosphere condition, two distinctly dissimilar mass patterns of carbon clusters were confirmed by varying the delay time of the ionization relative to the ablation. With shorter delay time, various size of C_n ($n \geq 6$) were observed. With longer delay time, on the contrary, merely the mass peak of C_{10}, along the weaker signal of C_{12}, was detected On the precise analysis of flight time, it was concluded that ablation products had split into two components with different velocities ("prompt" components and "delayed" components) due to the formation of dense boundary layer in the ablated plume. The peculiarly observed C_{10} in the delayed component was

assigned to monocyclic isomer with no reactive dangling bonds and special stability predicted theoretically.

For H_2 ambient gas case, various C_nH_m ($n \geq 3$, $m \leq 4$) and C_n ($n \geq 6$) were detected in the fast component. In the delayed component, however, only dihydrides $C_{2n}H_2$ (n=2–5) in addition to C_{10} were observed peculiarly. The dihydrides of delayed component were assigned to polyacetylenes. The observed coexistence with stable polyyne molecules and no hydrogenation also supported the especial stability and chemical inertness of C_{10}.

Further fine experiment with higher sensitivity and resolution revealed that the "delayed" component consists of two different components ("second" component and "third" component). It was clarified that the C_{10} observed in the "third" component was enhanced remarkably by heating the buffer gas up to 600 K. The enhancement suggested the relation of monocyclic carbon clusters with fullerenes formation.

It was concluded that, in this study, the ablation process of graphite was pursued by time-of-flight mass spectroscopy and non-emissive neutral products indiscernible by other experimental methods were identified successfully.

謝辞 (Acknowledgement in Japanese)

百瀬さん、若林さん、志田先生、鷲田先生、曽越さん、香月、伏谷、保科、森澤君、久間君、清水君、寺本君、宮本君、その他京大分子分光学研究室でお世話になったすべての皆様、本当にありがとうございました。

また、巣鴨や阪大の時からの友人たちにも多々励まされました。本当にありがとうございました。

最後に、僕の家族に心から感謝します。ありがとう。

というわけで、一区切りつきました。

みなさま今後ともよろしく。